Self-Assembled Monolayers Protected Metal Nanoparticles

3-D SAMs 3

organization of the monolayer

Chemically assisted organization of the monolayer

Asymmetric functionalization of Au NPs using a solid phase approach

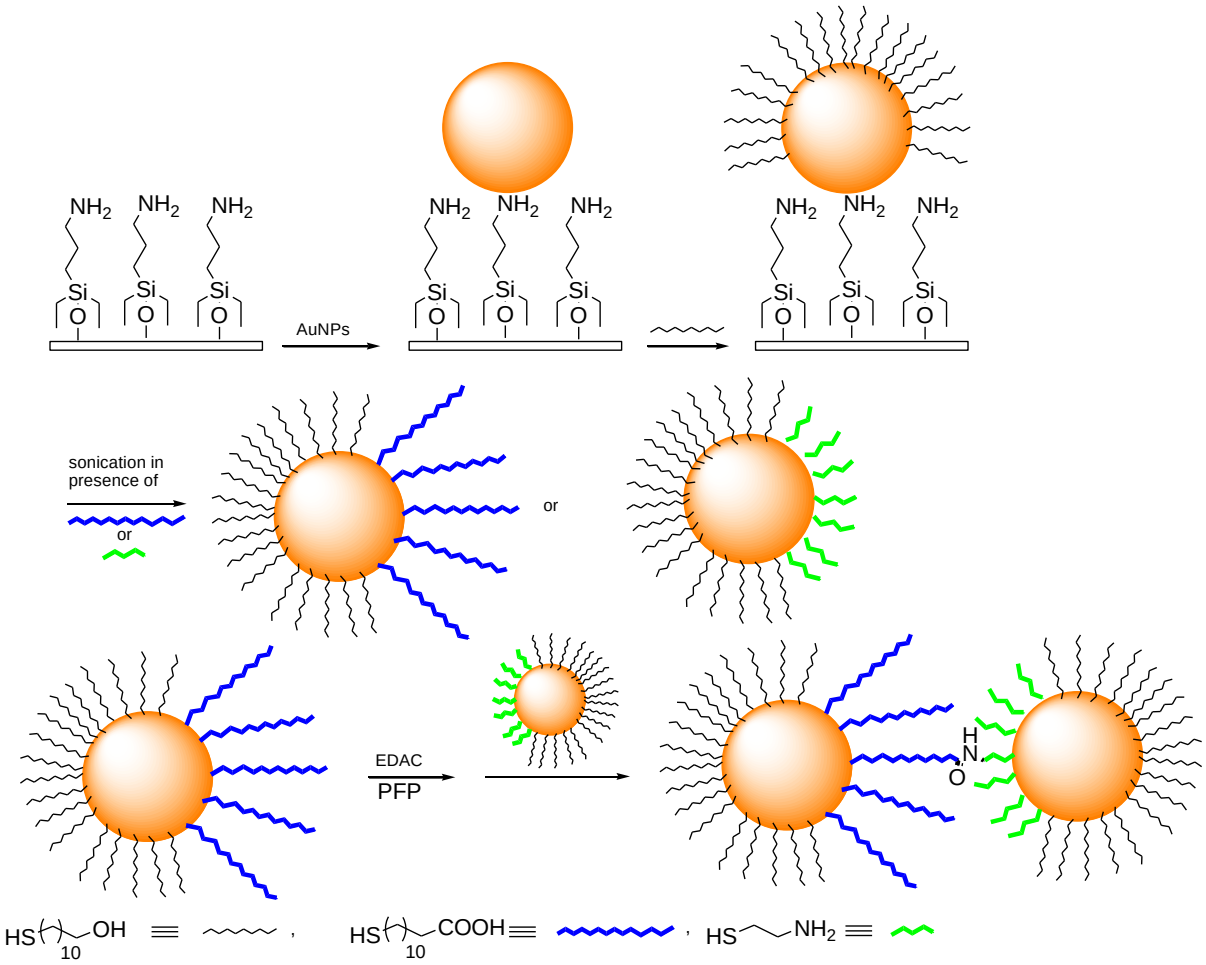

*R. Sardar, T. B. Heap and J. S. Shumaker-Parry, J. Am. Chem. Soc., 2007, **129**, 5356-5357*

organization of the monolayer

Chemically assisted organization of the monolayer

hydrogen bonding

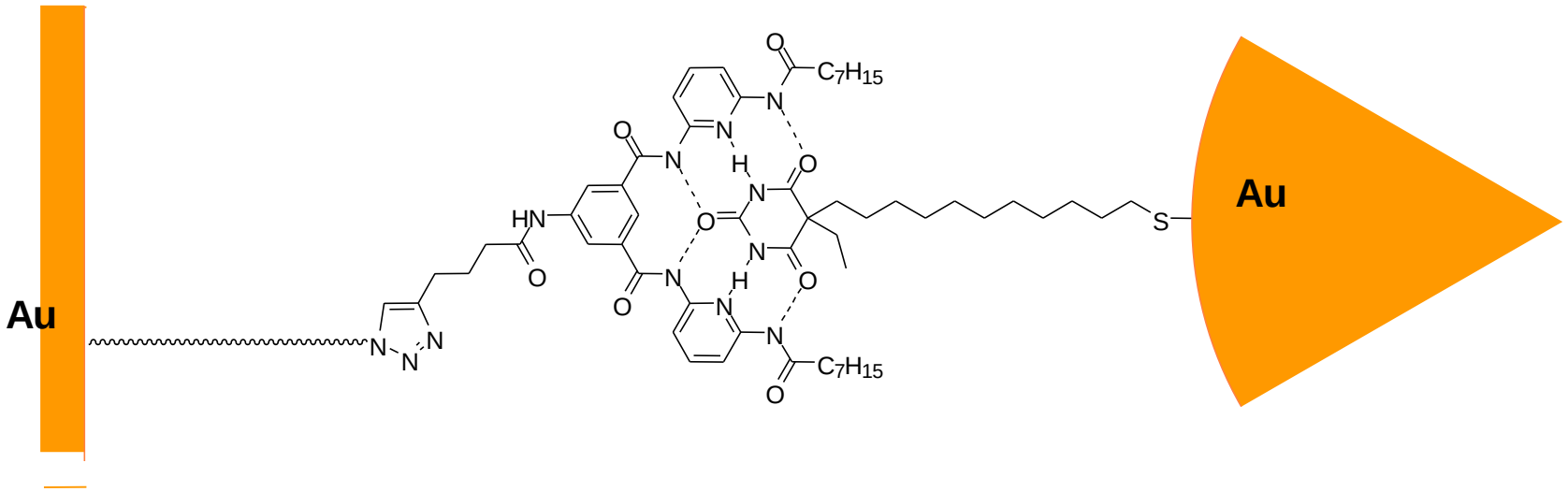

Self-assembling of gold NPs on surfaces mediated by Hamilton-type receptors.

*R. Zirbs, F. Kienberger, P. Hinterdorfer and W. H. Binder, Langmuir, 2005, **21**, 8414-8421.*

organization of the monolayer

Chemically assisted organization of the monolayer

hydrogen bonding

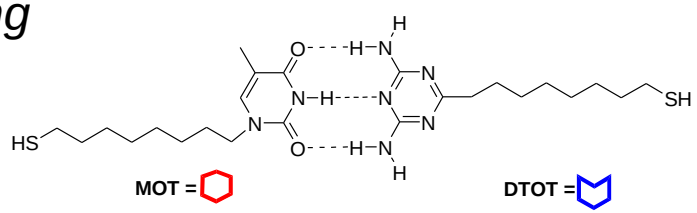

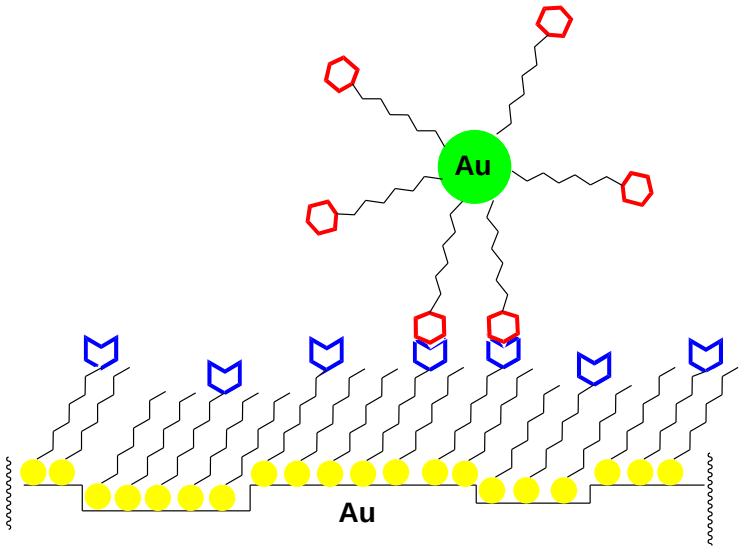

Au_{55} clusters functionalized with MOT molecules are immobilized by molecular recognition onto a mixed SAM composed of n-heptanethiol and DTOT molecules.

*C. R. van den Brom, I. Arfaoui, T. Cren, B. Hessen, T. T. M. Palstra, J. T. M. de Hosson and P. Rudolf, Adv. Funt. Mater., 2007, **17**, 2045-2052.*

organization of the monolayer

Chemically assisted organization of the monolayer

segregation driven by an external template

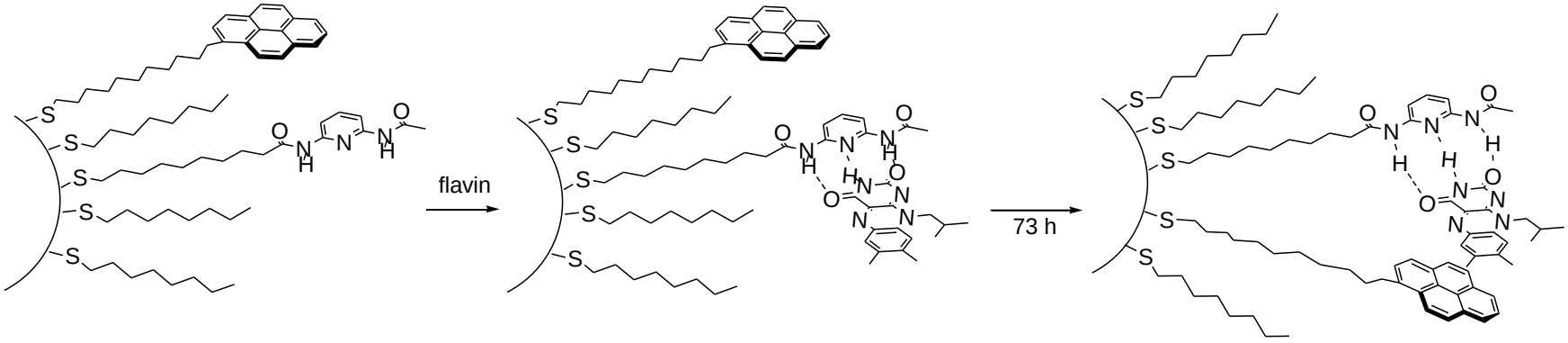

Schematic illustration of reorganization of the monolayer upon flavin addition driven by π-stacking.

*A. K. Boal and V. M. Rotello, J. Am. Chem. Soc., 2000, **122**, 734-735.*

organization of the monolayer

Chemically assisted organization of the monolayer

segregation driven by an external template

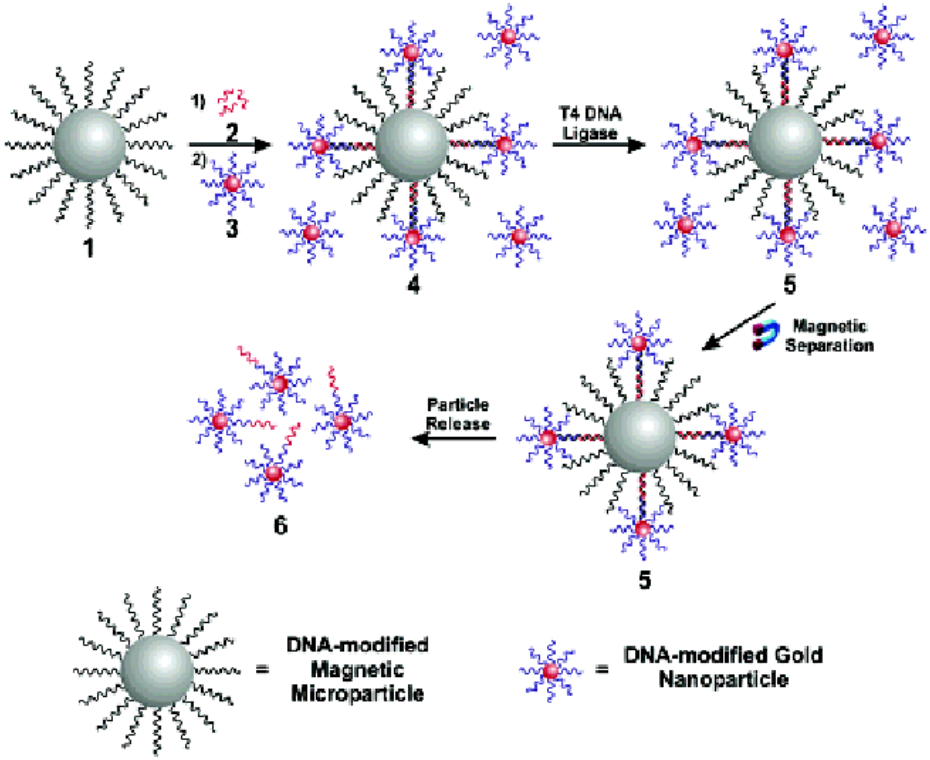

Anisotropic functionalization of gold NPs by using a magnetic sphere as a geometrical restriction template.

*X. Xu, N. L. Rosi, Y. Wang, F. Huo and C. A. Mirkin, J. Am. Chem. Soc., 2006, **128**, 9286-9287.*

organization of the monolayer

organization of the monolayer at interfaces

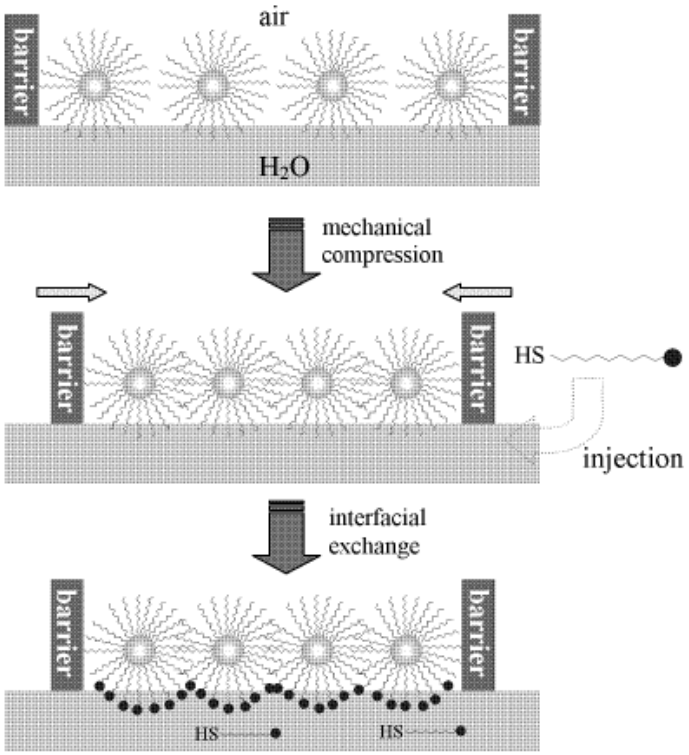

Schematic illustration of the preparation of Janus nanoparticles based on the Langmuir technique.

*S. Pradhan, L.-P. Xu and S. Chen, Adv. Funct. Mater., 2007, **17**, 2385-2392.*

Monovalent gold nanoparticles

Electrophoretic Isolation of Discrete Au Nanocrystal/DNA Conjugates

D. Zanchet, C. M. Micheel, W. J. Parak, D. Gerion, A. P. Alivisatos, *Nano Lett.* **2001**, *1*, 32.

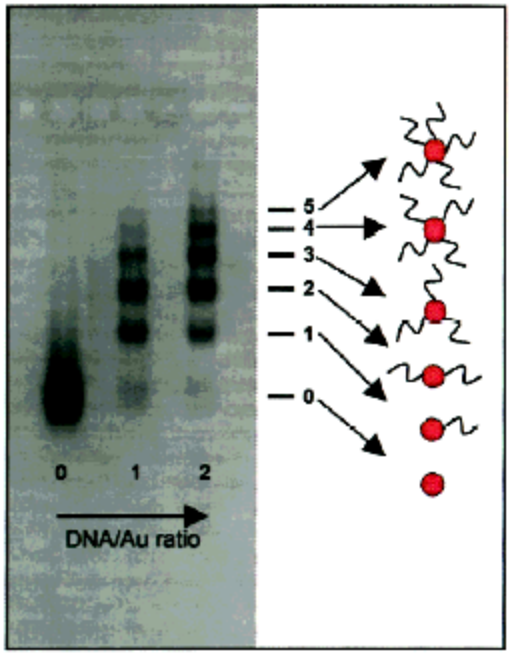

Figure 1. Electrophoretic mobility of 5 nm Au/100b HS-ssDNA conjugates (3% gel). The first lane (left to the right) corresponds to 5 nm particles (single band). When ~1 equiv of DNA is added to the Au particles (second lane), discrete bands appear (namely **0**, **1**, **2**, **3**, ...). When the DNA amount is doubled (third lane), the intensity of the discrete bands change and additional retarded bands appear (**4**, **5**). Because of the discrete character, each band can be directly assigned to a unique number of DNA strands per particle.

Monovalent gold nanoparticles

Synthesis of Monofunctionalized Gold Nanoparticles by Fmoc Solid-Phase Reactions

K.-M. Sung, D. W. Mosley, B. R. Peelle, S. Zhang, J. M. Jacobson

J. Am. Chem. Soc. **2004**, *126*, 5064

Scheme 1. Synthesis of Lys-Monofunctionalized Gold Nanoparticles[a]

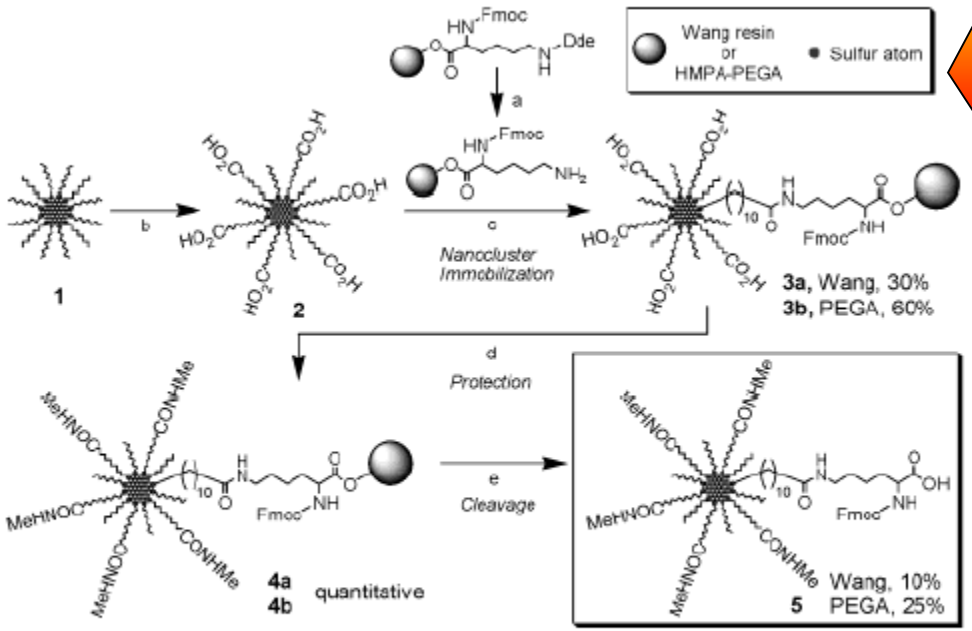

[a] Reagents and conditions: (a) $H_2NNH_2 \cdot H_2O$/DMF (2% v/v), DIPEA/DMF (10% v/v). (b) $HS(CH_2)_{10}CO_2H$ (excess), THF. (c) DIC (excess), DMF/THF (10% v/v) room temperature, 24 h. (d) $MeNH_2$, DIC (excess), DMF/THF, room temperature, 12 h. (e) 60% TFA, 2.5% TIS, 2.5% H_2O, 35% DMF, 24 h.

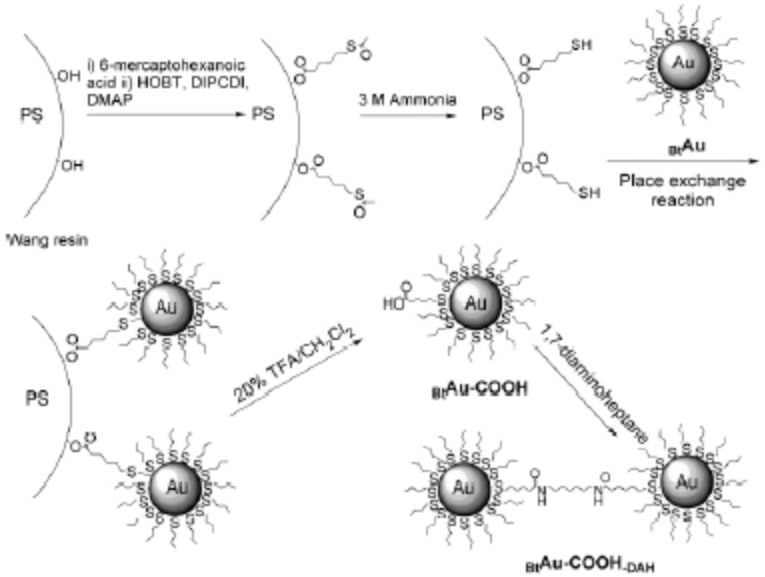

Scheme 1 HOBT, 1-hydroxybenzotriazole; DIPCDI, 1,3-diisopropylcarbodiimide; DMAP, 4-(dimethylamino)pyridine.

Controlled functionalization of gold nanoparticles through a solid phase synthesis approach

J. G. Worden, A. W. Shaffer, Q. Huo, *Chem. Commun*. **2004**, 518.

Monovalent gold nanoparticles

A Generic Approach to Monofunctionalized Protein-Like Gold Nanoparticles Based on Immobilized Metal Ion Affinity Chromatography

R. Lvy, Z. Wang, L. Duchesne, R. C. Doty, A. I. Cooper, M. Brust, D. G. Fernig, *ChemBioChem* **2006**, *7*, 592.

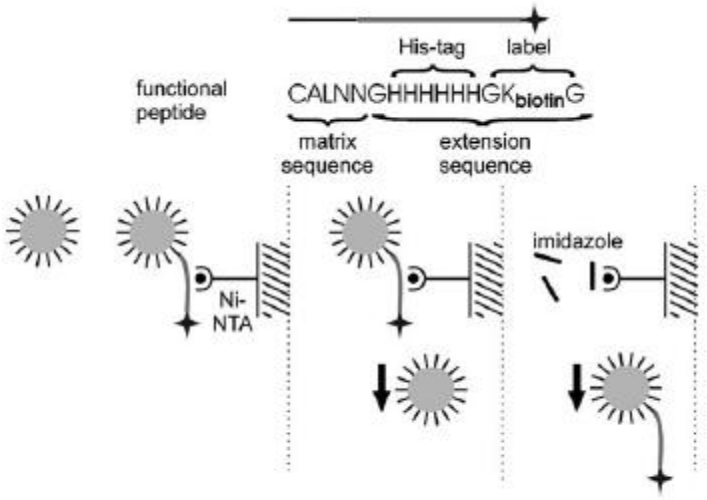

Figure 1. Design of the functional peptide and separation principle of labelled and unlabelled peptide-capped NPs by using IMAC.

IMAC = metal ion affinity chromatography

Divalent gold nanoparticles

Divalent Metal Nanoparticles

Gretchen A. DeVries, Markus Brunnbauer, Ying Hu, Alicia M. Jackson, Brenda Long, Brian T. Neltner, Oktay Uzun, Benjamin H. Wunsch, Francesco Stellacci*

19 JANUARY 2007 VOL 315 SCIENCE 358

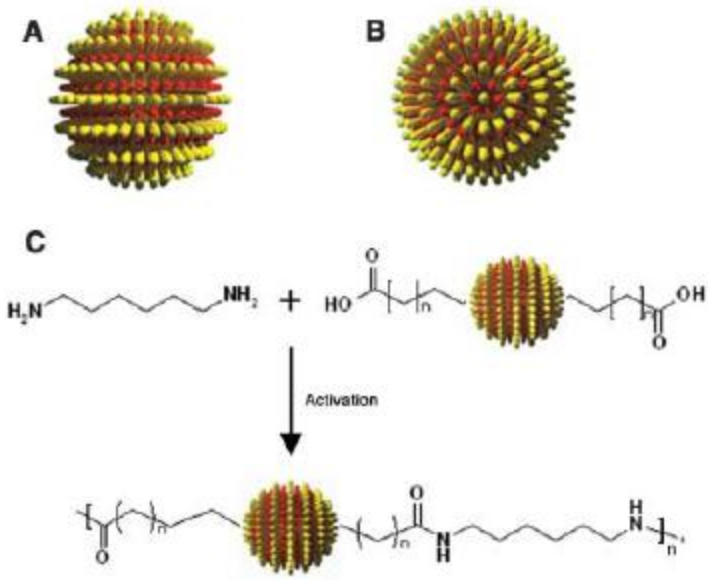

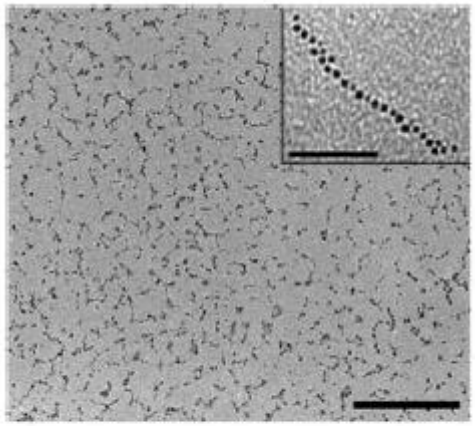

Fig. 2. TEM images of chains that compose the precipitate obtained when MUA pole-functionalized rippled NPs are reacted with DAH in a two-phase reaction. Scale bars 200 nm, inset 50 nm.

tethered nano building blocks

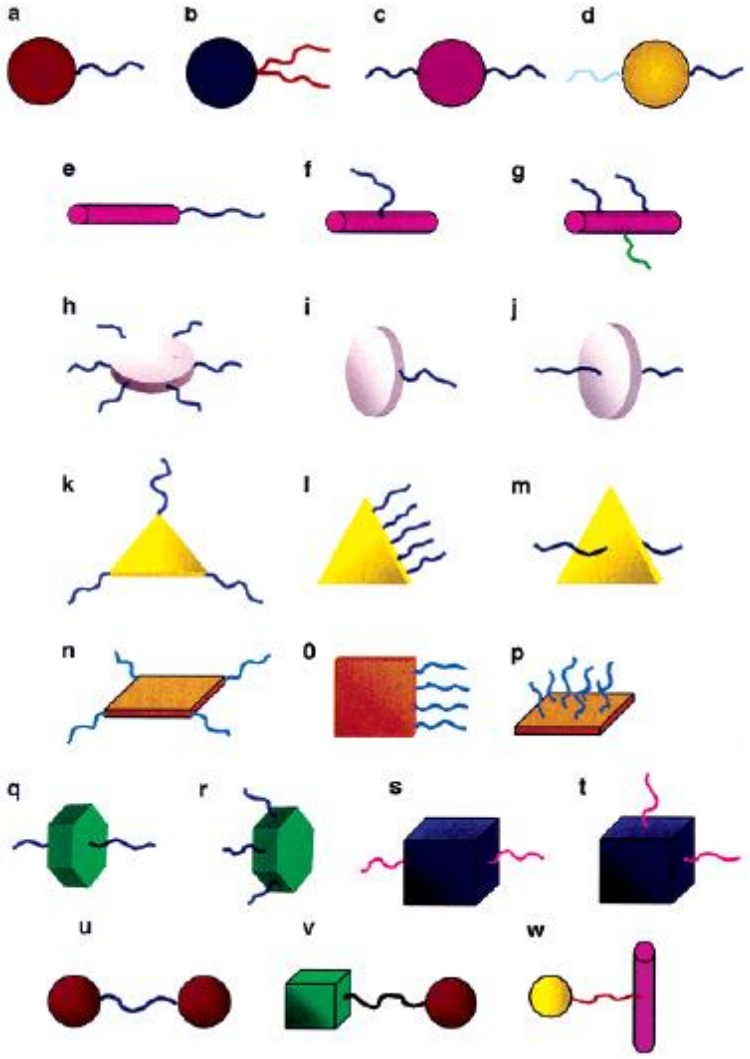

ANISOTROPIC METAL NANOPARTICLES

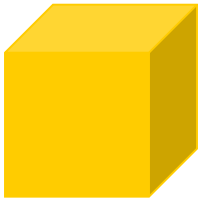

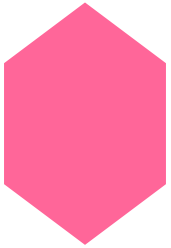

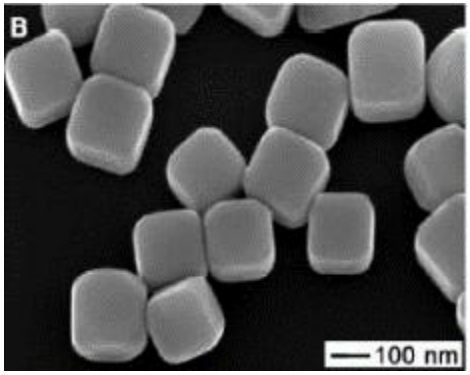

SEM image of Silver Nanocubes[1]

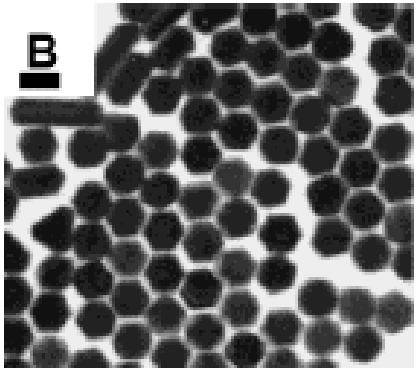

TEM images of Au nanoparticles. Scale 100 nm[2]

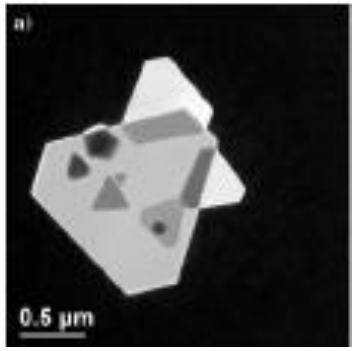

HAADF image of Au nanoparticles: synthesized @ 100°C[3]

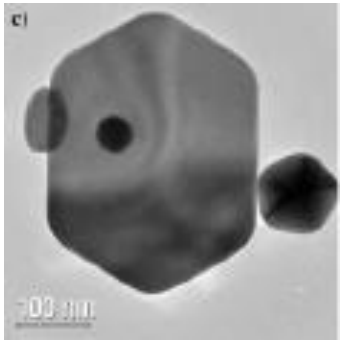

TEM image of particles sinthesized @ 190°C[3]

gold nanorods

Seed-mediated Growth in Solution

1. Chemical reduction of a metal salt with strong reducing agent ($NaBH_4$),
2. Use of a capping agent to prevent particle growth (citrate),
3. Addition of the seeds to a solution that contains more metal salt, a weak reducing agent (AA) and a rodlike micellar template (cetyltrimethylammonium bromide, CTAB).

Aspect ratio is controlled by the ratio of metal seed to metal salt.

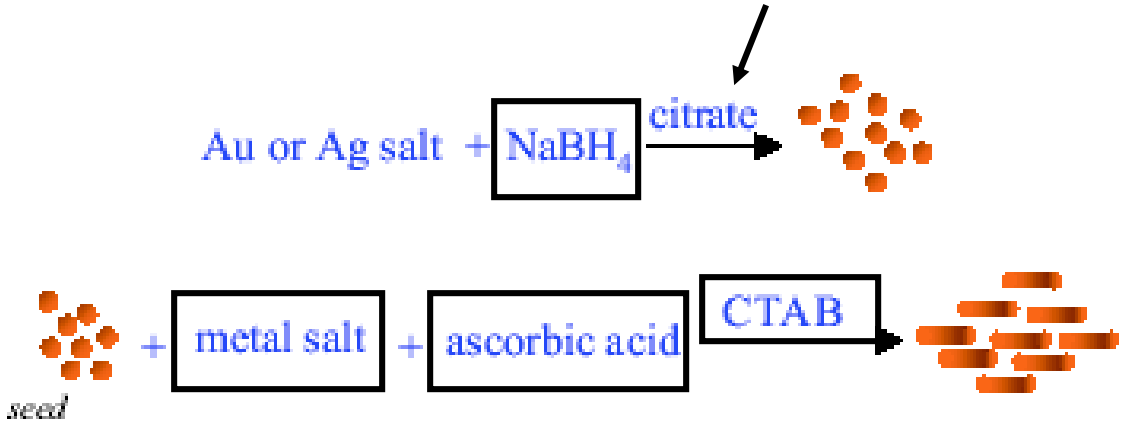

C.J.Murphy, N.R.Jana, *Adv.Mater.* 2002, 14 (80-82)

gold nanorods

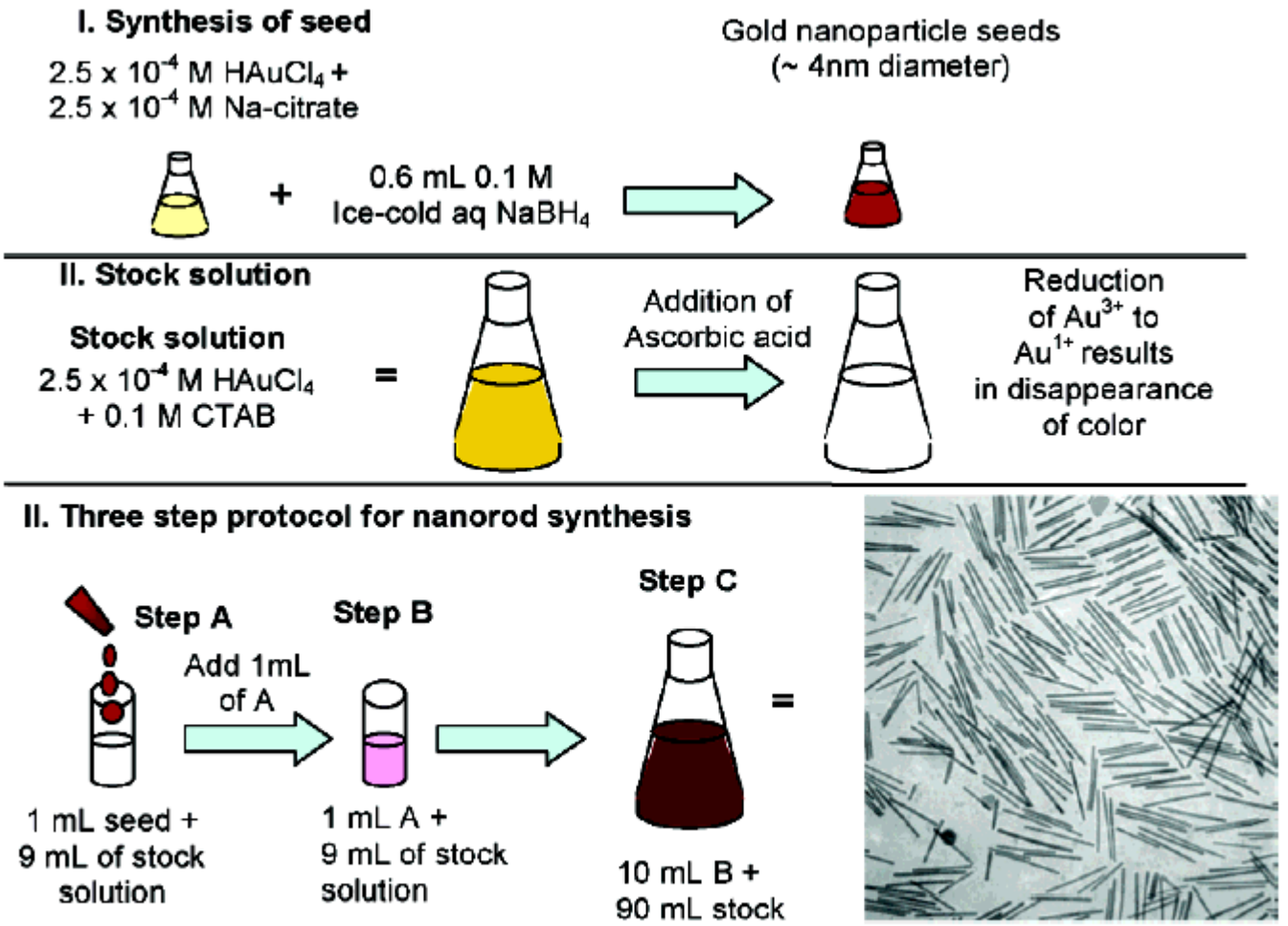

Figure 2. Seed-mediated growth approach to making gold and silver nanorods of controlled aspect ratio. The specific conditions shown here, for 20 mL volume of seed solution, lead to high-aspect ratio gold nanorods. (bottom right) Transmission electron micrograph of gold nanorods that are an average of 500 nm long.

Nikoobahkt and El-Sayed, *Chem. Mater.* **2003**, *15*, 1957;
Sau and Murphy, *Langmuir* **2004**, *20*, 6414.

gold nanorods

Influence of the reaction parameters

✓ Effect of the Seed Concentration

An **increase** in the **$[Au]_{seed}$** **decreased** the **rod length** for a given concentration of Au^{3+}.

✓ Effect of AA concentration

The **rod length decreases** with an **increase in [AA]** keeping all other conditions the same.

✓ Effect of $AgNO_3$

When **silver nitrate** is **not used** nanorods are obtained in **low yield** and quite **long**.

✓ Effect of $[Au^{3+}]$

The **less** quantity of **Au^{3+} ions** per seed particle available the **short** are the nanorods.

✓ Effect of [CTAB]

Lower CTAB concentrations can lead to **non-rod-shaped** particles.

gold nanorods

Variation in the absorption of visible light

Short aspect ratio Au nanorods are especially interesting because of their optical properties: they exhibit tranverse and longitudinal plasmon bands.

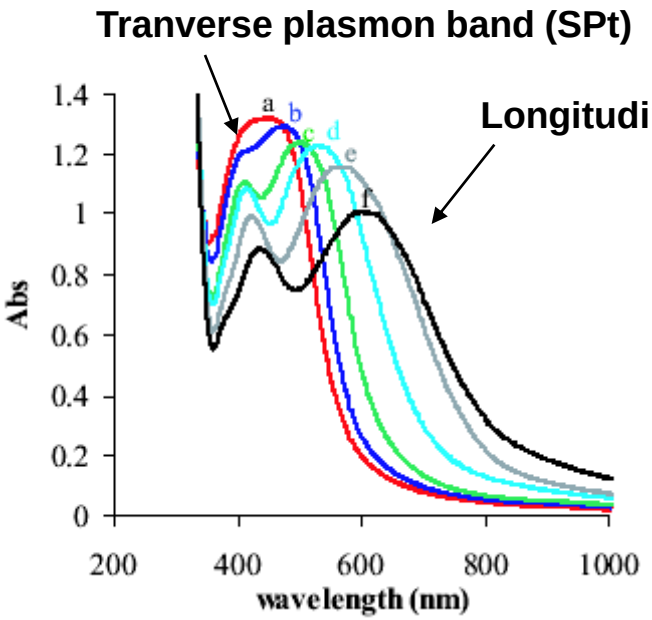

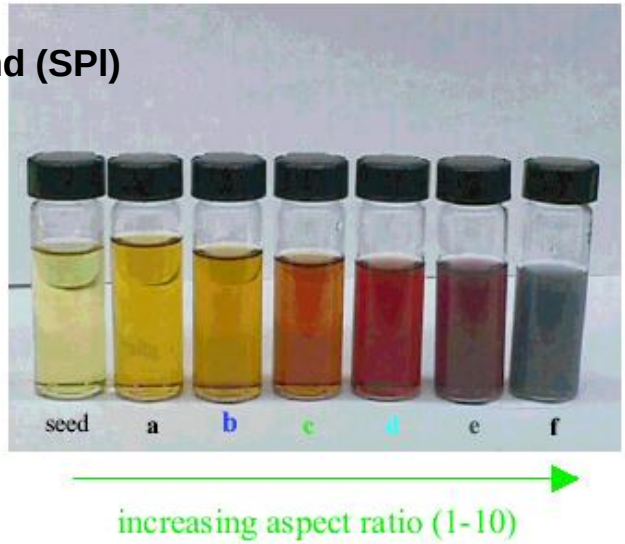

Aspect ratio: the length of the major axis divided by the width of the minor axis.

The larger the aspect ratio, the more red-shifted the longitudinal plasmon band.

gold nanorods

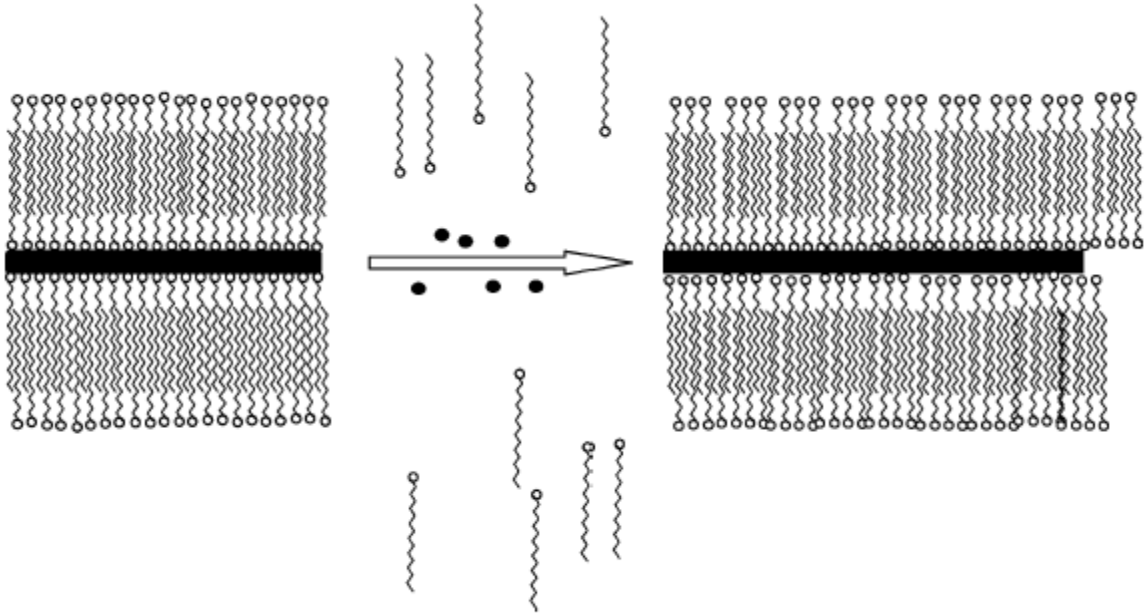

Figure 7. Cartoon illustrating "zipping": the formation of the bilayer of CnTAB (squiggles) on the nanorod (black rectangle) surface may assist nanorod formation as more gold ion (black dots) is introduced. Reproduced from ref 104 with permission.

gold nanorods

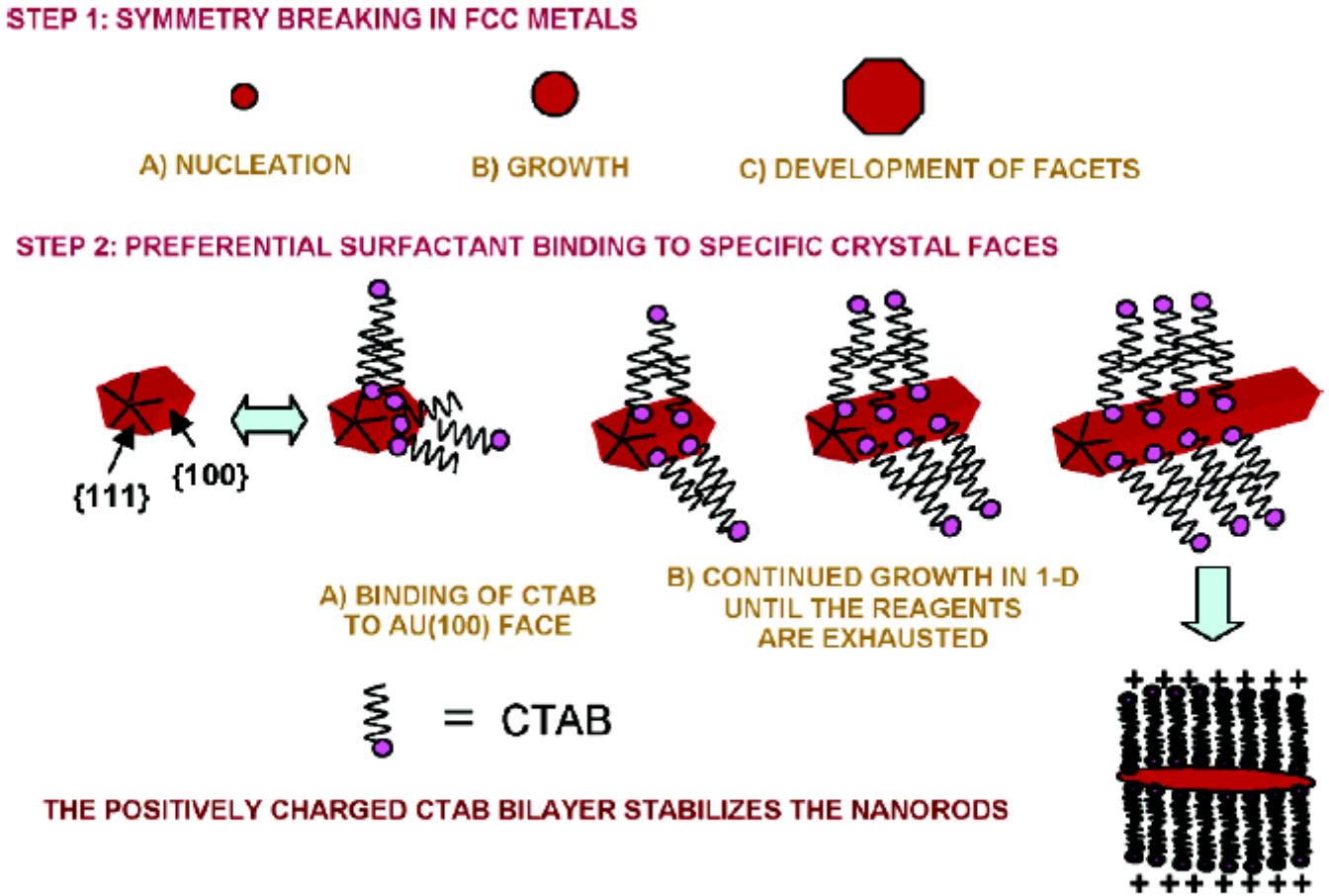

Figure 8. Proposed mechanism of surfactant-directed metal nanorod growth. The single crystalline seed particles have facets that are differentially blocked by surfactant (or an initial halide layer that then electrostatically attracts the cationic surfactant). Subsequent addition of metal ions and weak reducing agent lead to metallic growth at the exposed particle faces. In this example, the pentatetrahedral twin formation leads to Au {111} faces that are on the ends of the nanorods, leaving less stable faces of gold as the side faces, which are bound by the surfactant bilayer.

ANISOTROPIC METAL NANOPARTICLES

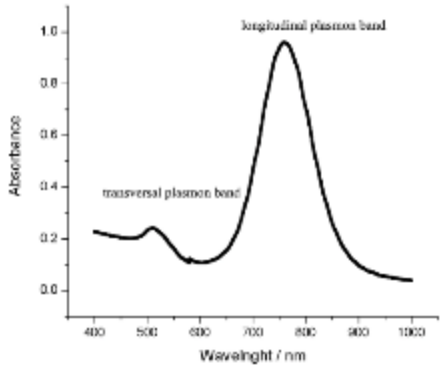

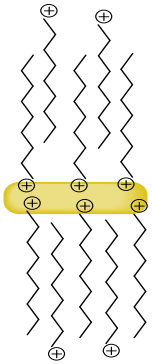

Figure 1. UV spectra of an aqueous solution of gold nanorods.

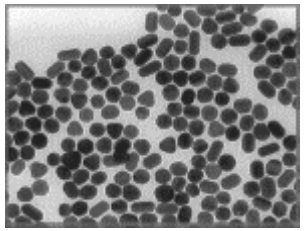

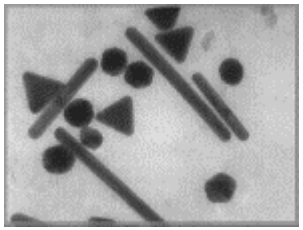

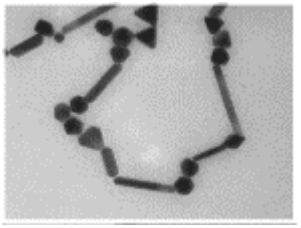

no $AgNO_3$

Silver-Assisted Synthesis of Gold Nanorods: the Relation between Silver Additive and Iodide Impurities

Small **2018**, *14*, 1703879

Sarah Jessl, Moritz Tebbe, Luca Guerrini, Andreas Fery, Ramon A. Alvarez-Puebla,* and Nicolas Pazos-Perez**

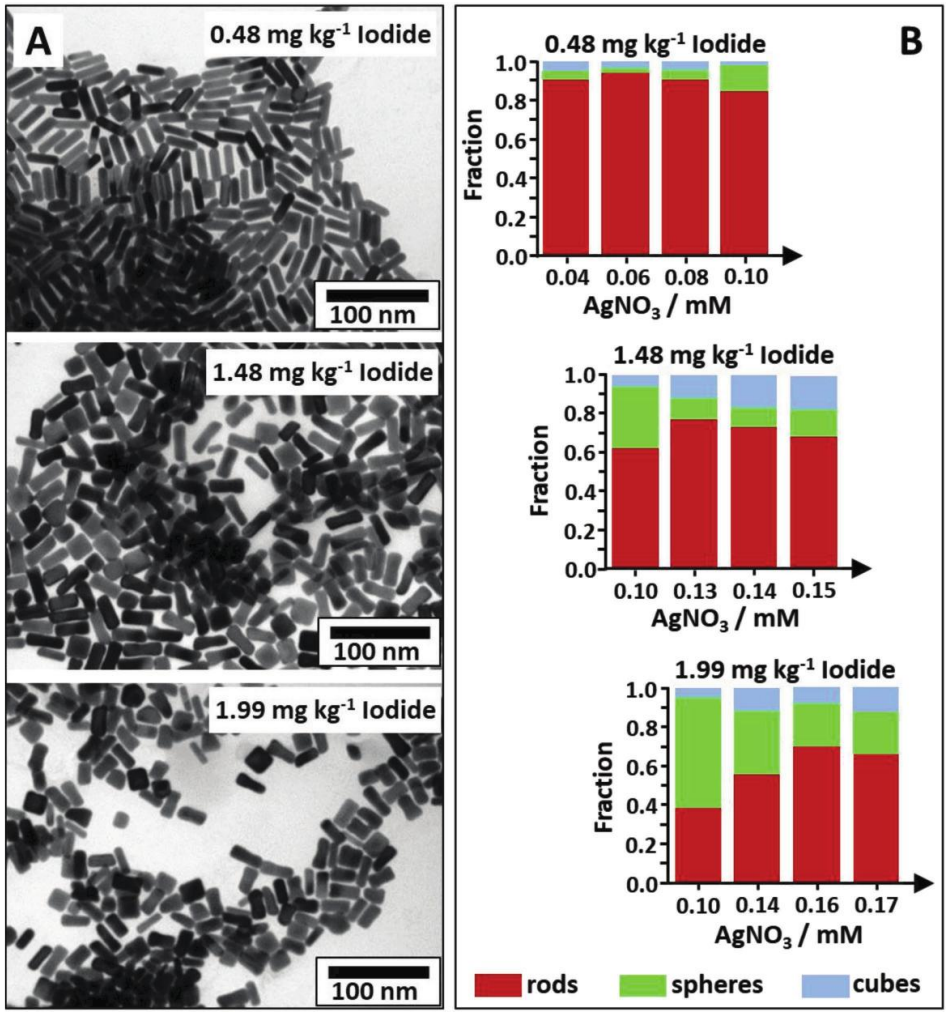

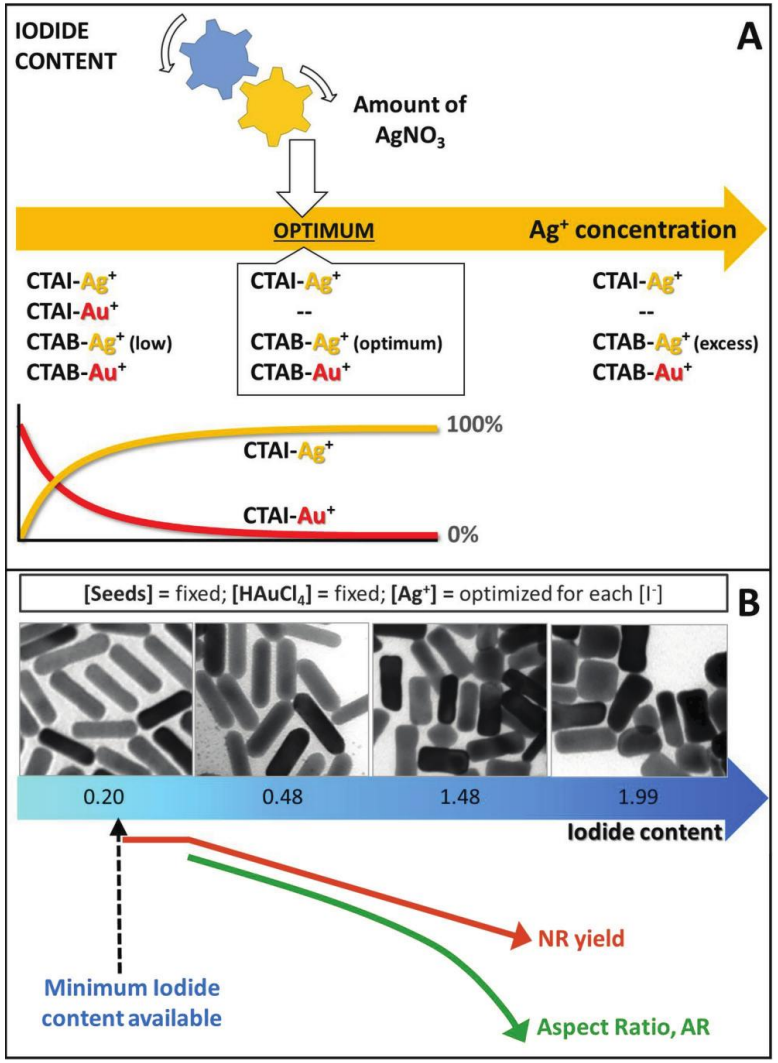

gold nanorods - functionalization

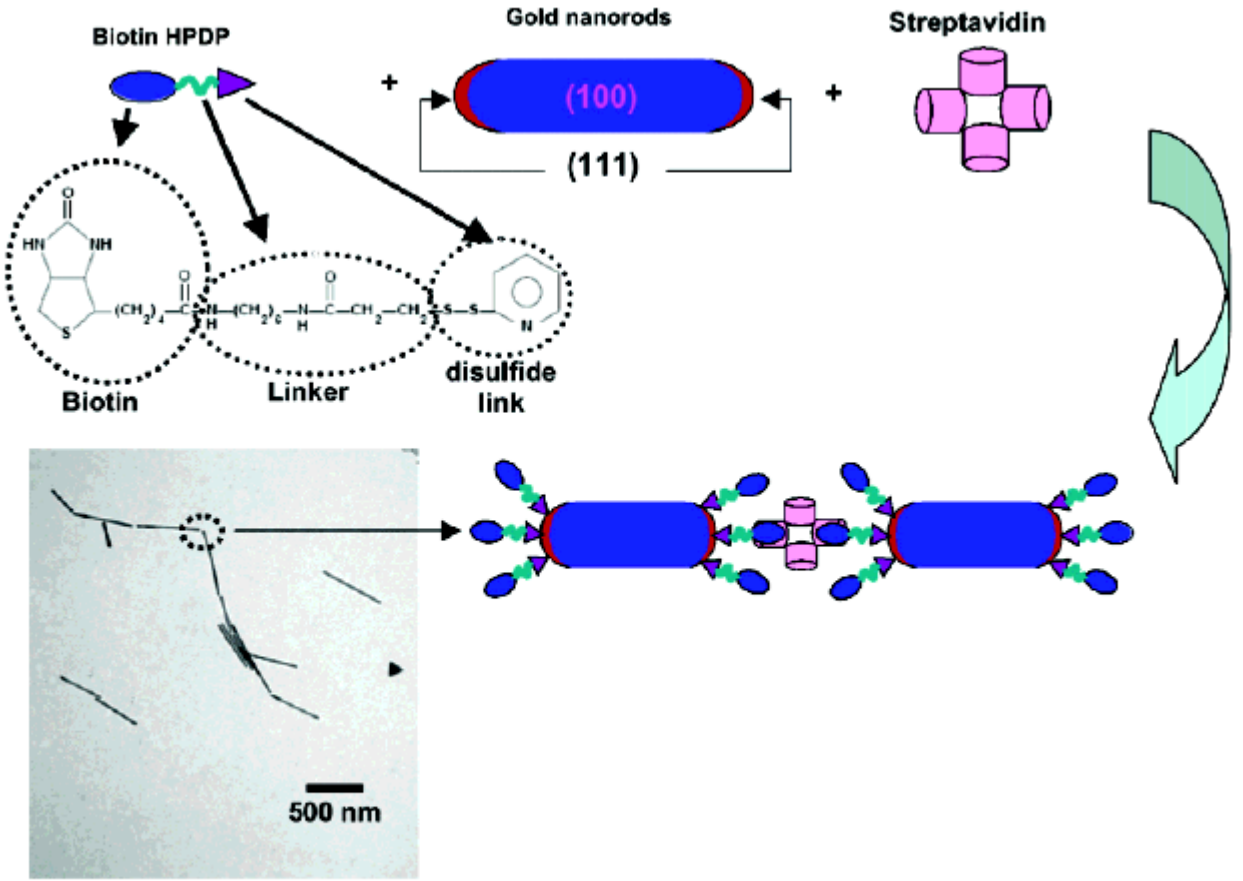

Figure 9. Cartoon of biotin-streptavidin assembly of gold nanorods; a biotin disulfide is added to biotinylate the rods, and subsequent addition of streptavidin causes noncovalent assembly. Inset: transmission electron micrograph of gold nanorod-streptavidin assemblies. The original data are from ref 86.

gold nanorods - functionalization

Scheme 1. Scheme Showing the Process Involved in the Click Chemistry Reaction of Azide-Functionalized Gold Nanorods with Acetylene-Functionalized Trypsin

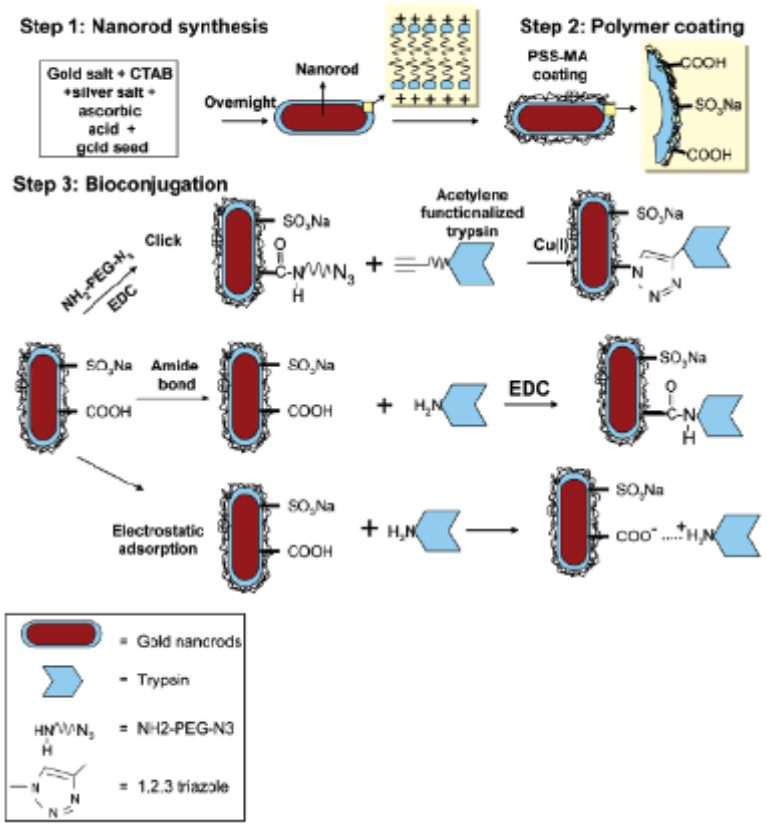

ANISOTROPIC METAL NANOPARTICLES

Branched structures: Tripods & Tetrapods

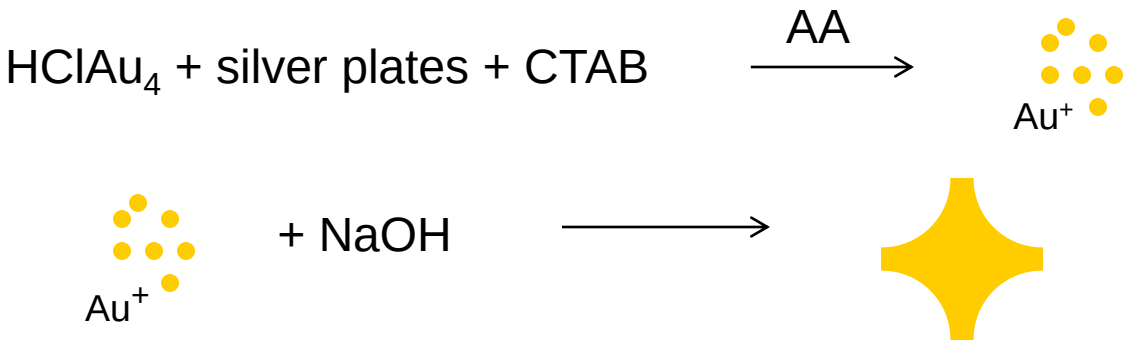

The forced reduction of gold by ascorbic acid through the addition of NaOH is the key step for particle branching.

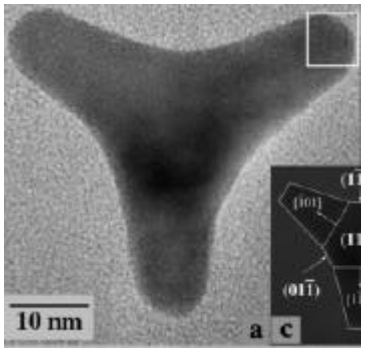

TEM image of a regular tripod nanocrystal

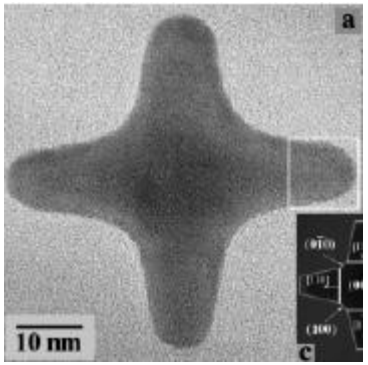

TEM image of a tetrapod nanocrystal

J.Am.Chem.Soc. 2003, 125, 16186-16187

ANISOTROPIC METAL NANOPARTICLES

From Ag nanocubes to Au nanoboxes

When Silver nanocubes are treated with a gold salt, an oxidation-reduction reaction ensues. In this reaction, the silver nanocubes serve as a sacrificial hard template to make hollow crystalline gold nanoboxes.

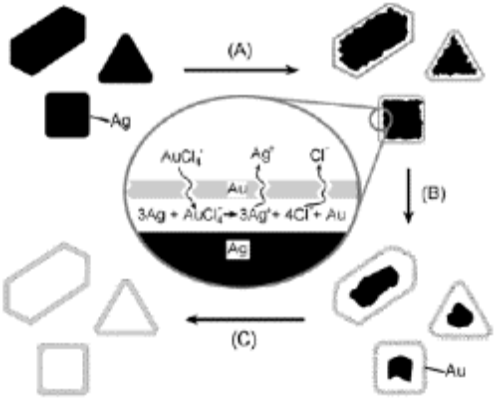

$$3\,Ag(s) + HAuCl_4(aq) \longrightarrow Au(s) + 3AgCl(aq) + HCl(aq)$$

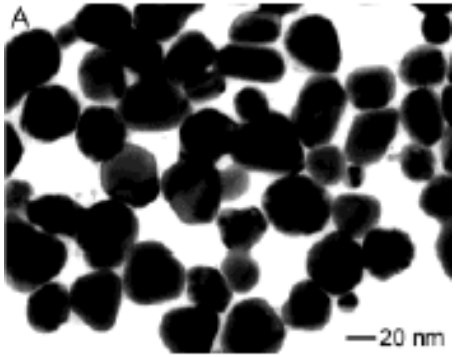

TEM image of silver nanoparticles synthesized using the polyol process.

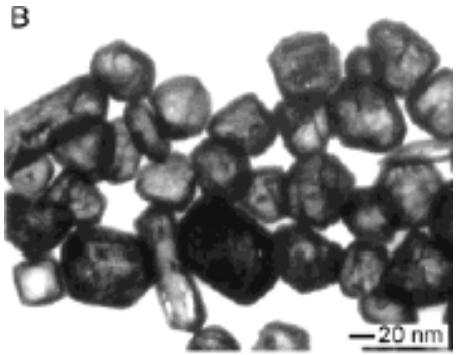

TEM image of gold nanoshells.

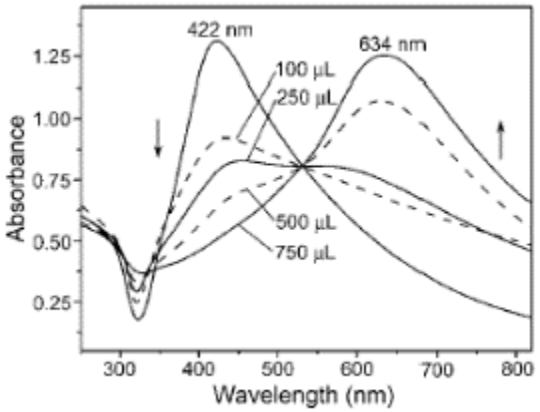

UV-vis absorption spectra of an aqueous dispersion of Ag nanoparticles.

Y. Sun, B.T. Mayers and Y. Xia, *Nano Letters,* **2002**, 2, 481- 485

Au nanoboxes

By controlling the molar ratio between Ag and $HAuCl_4$, the gold nanocages could be tuned to display surface plasmon resonance peaks around 800 nm, a wavelength commonly used in optical coherence tomography (OCT) imaging.

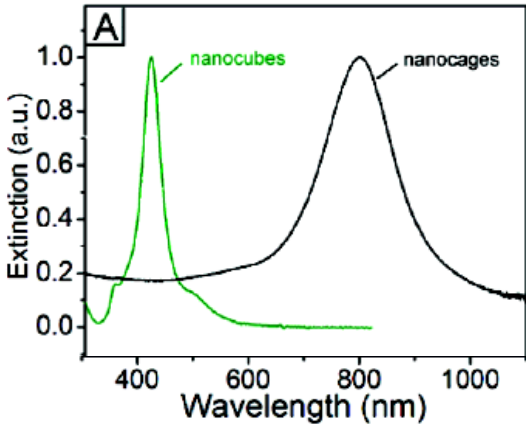

UV exctinction spectra recorded from solutions of Ag nanocubes and Au nanocages.

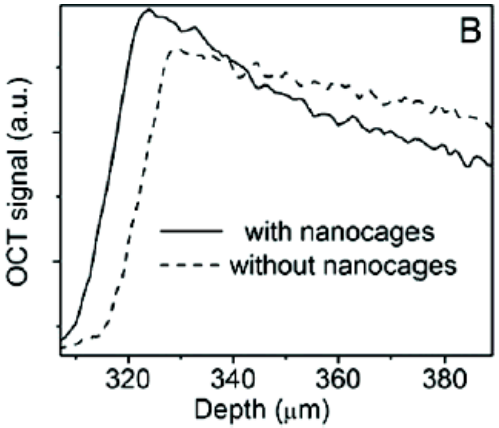

Plot of the OCT signals on a long scale as a function of depth.

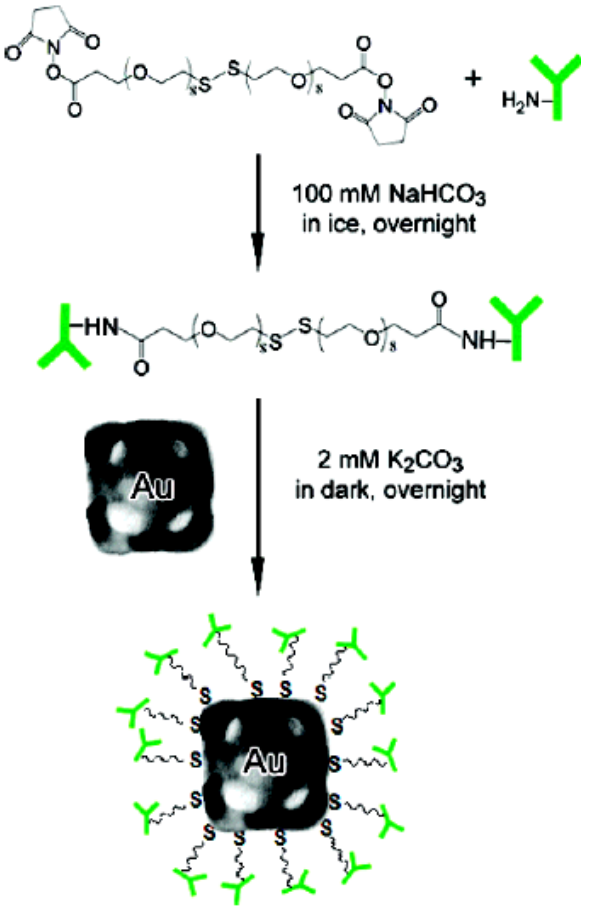

Gold nanocages functionalized with tumor-specific antibodies.

J.Chen, Y.Xia et al, *Nano Lett*ers, 2005, 5, 473-477.

Nanoparticles - Applications

- *NP for gene and drug delivery*
- *DNA sensing*
- *proteins sensing*
- *recognition and multivalency*
- *imaging*
- *catalysis*
- *new materials*

Nanoparticle-based Sensors

hydrogen bonds drive self-assembly

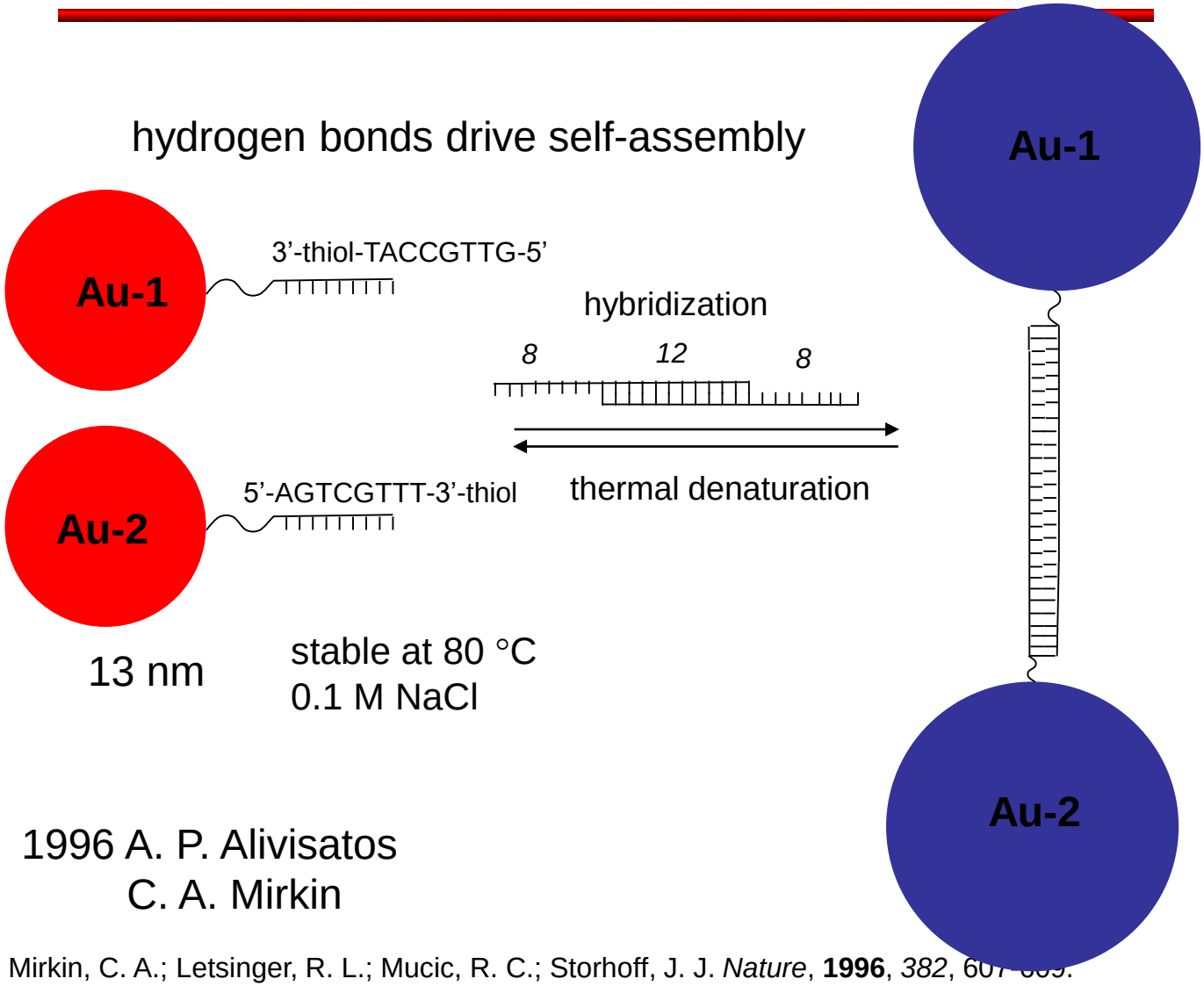

13 nm

stable at 80 °C
0.1 M NaCl

1996 A. P. Alivisatos
C. A. Mirkin

Mirkin, C. A.; Letsinger, R. L.; Mucic, R. C.; Storhoff, J. J. *Nature*, **1996**, *382*, 607-609.
Alivisatos, A. P.; Johnsson, K. P.; Peng, X.; Wilson, T. E.; Loweth, C. J.; Bruchez, M. P. Jr.; Schultz, P. G. *Nature*, **1996**, *382*, 609-611.

Nanoparticle-based Sensors

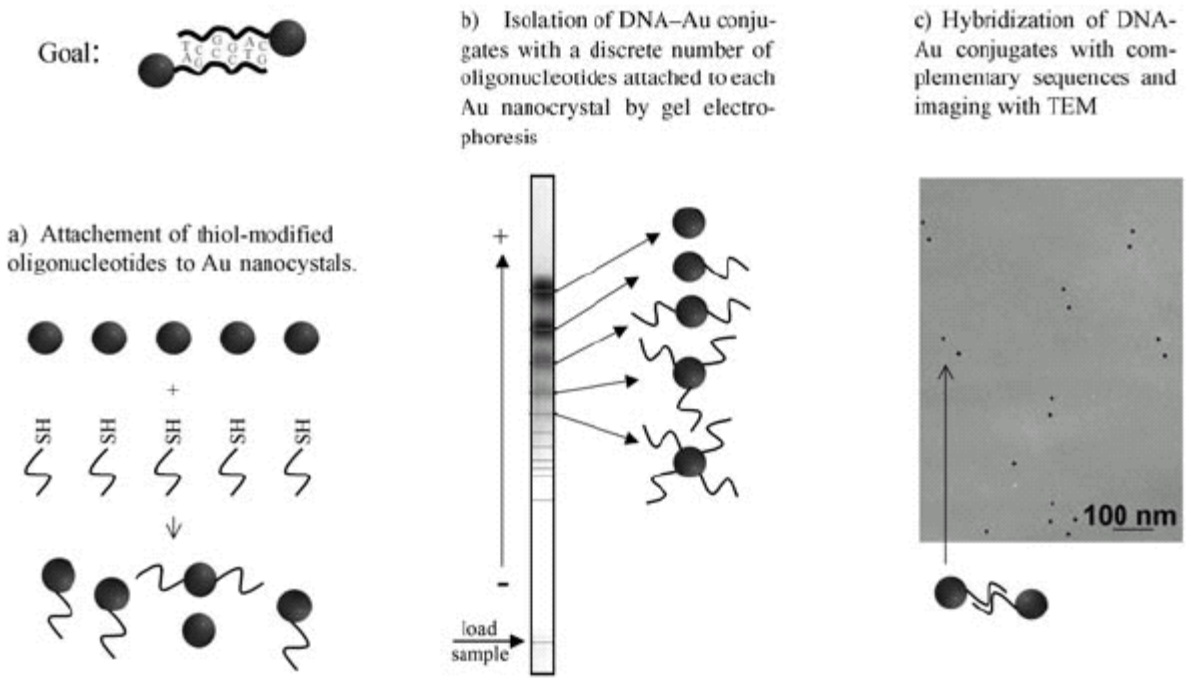

Figure 7. Forming DNA-meditated dimers of Au nanoparticles requires each nanoparticle to be functionalized with one oligonucleotide, with both oligonucleotides being complementary to each other. a) When phosphine- (or citric acid) stabilized Au nanoparticles and thiol-modified oligonucleotides react, DNA binds with its thiol group to the Au surface. However, even for 1:1 mixtures of DNA and Au, Au nanoparticles with more or less than one bound oligonucleotide will result; b) Au nanoparticles with a different number of DNA molecules bound per particle can be sorted by gel electrophoresis (image adapted from ref. [87]). Individual bands of nanoparticles with a discrete number of DNA molecules per particle can be observed and extracted from the gel; c) Au nanoparticles with one DNA molecule can be mixed with another solution of Au nanoparticles modified with a complementary DNA sequence. The single-stranded DNA molecules hybridize to a double strand, thus connecting the Au nanoparticles. The resulting dimers can be observed by TEM imaging (the Au-nanoparticle dimers shown comprise two 10-nm-diameter Au nanocrystals; the DNA molecules cannot be seen by TEM). Image courtesy of D. Zanchet et al.[7]

Alivisatos, A. P.; Johnsson, K. P.; Peng, X.; Wilson, T. E.; Loweth, C. J.; Bruchez, M. P. Jr.; Schultz, P. G. *Nature*, **1996**, *382*, 609-611.

Nanoparticle-based Sensors

selective colorimetric detection system for polynucleotides

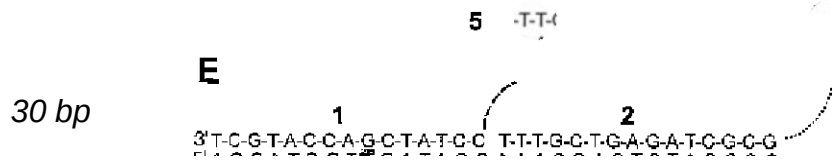

thermal transition associated with the color change

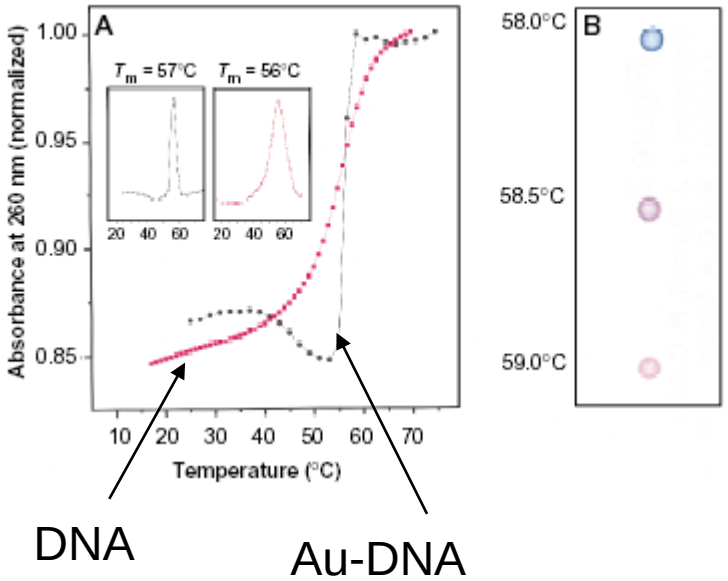

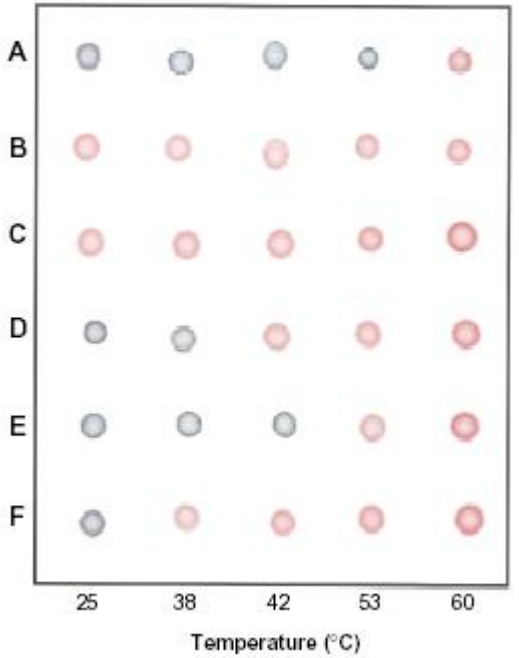

Selective polynucleotide detection for the target probes : (**A**) complementary target; (**B**) no target; (**C**) complementary to one probe; (**D**) a 6-bp deletion; (**E**) a 1-bp mismatch; and (**F**) a 2-bp mismatch. Nanoparticle aggregates were prepared in a 600-μl thin-walled Eppendorf tube by addition of 1 μl of a 6.6μM oligonucleotide target to a mixture containing 50 μl of each probe (0.06 μM final target concentration). The mixture was frozen (5 min) in a bath of dry ice and isopropyl alcohol and allowed to warm to room temperature. Samples were then transferred to a temperature controlled water bath, and 3-μl aliquots were removed at the indicated temperatures and spotted on a C_{18} reverse phase plate.

Elganian, R.; Storhoff, J.J.; Mucic, R. C.; Letsinger, R. L.; Mirkin, C. A. *Science* **1997**, *277*, 1078-1081.

Nanoparticle-based Sensors

selective colorimetric detection system for polynucleotides

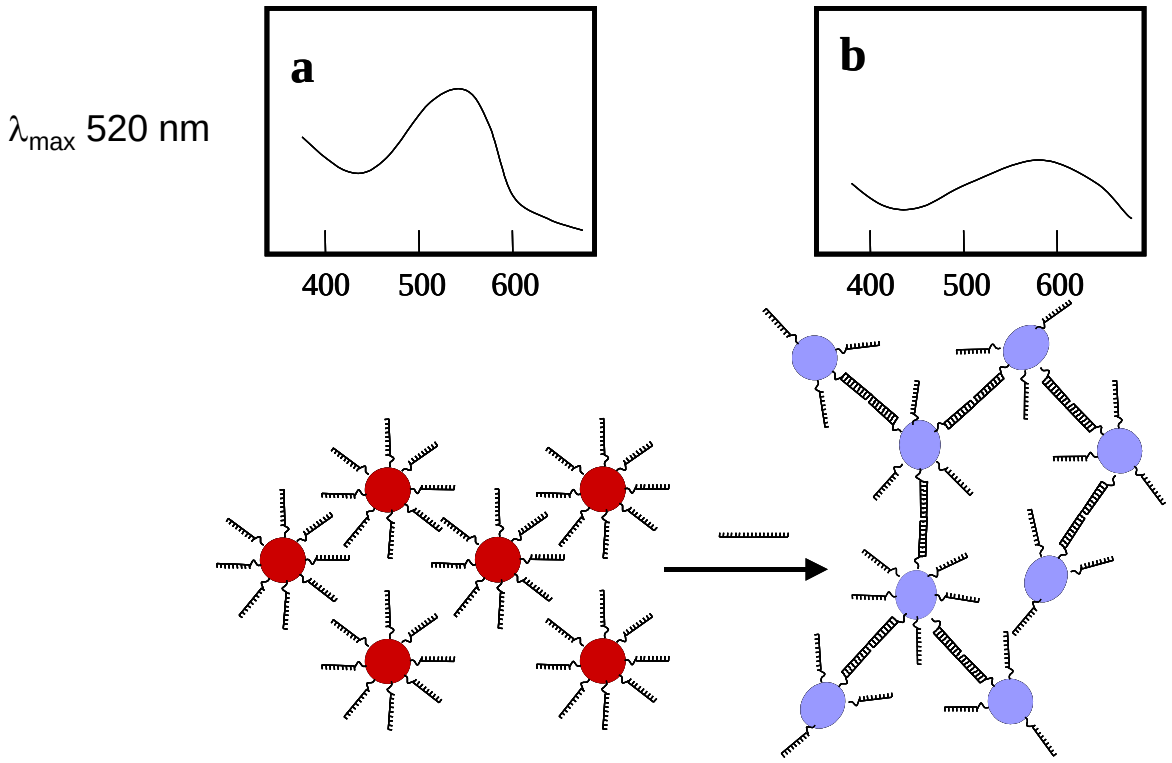

very sensitive: 10 femtomoles of polynucleotide could be detected

Elganian, R.; Storhoff, J.J.; Mucic, R. C.; Letsinger, R. L.; Mirkin, C. A. *Science* **1997**, *277*, 1078-1081.

Nanoparticle-based Sensors

scanometric DNA array detection

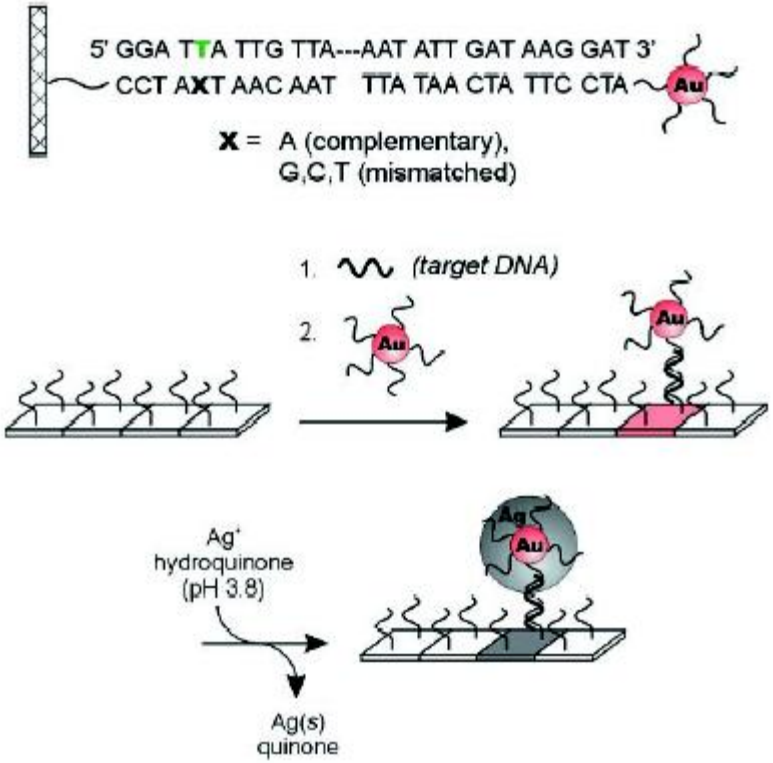

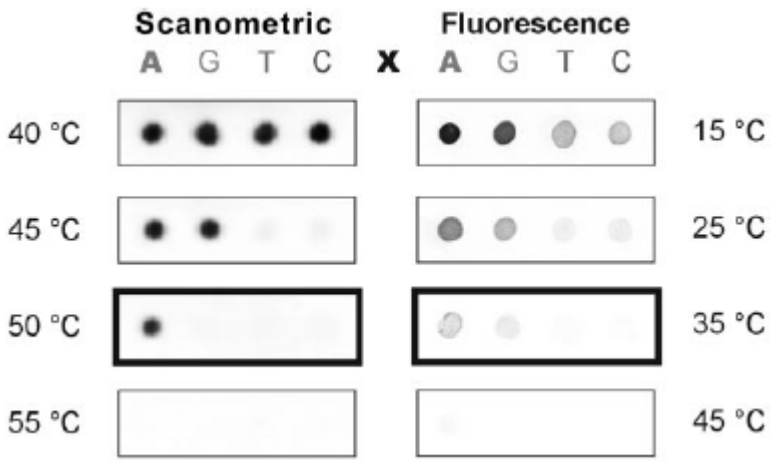

Taton, T. A.; Mirkin, C. A.; Letsinger, R. L. *Science* **2000**, *289*, 1757-1760.

Nanoparticle-based Sensors

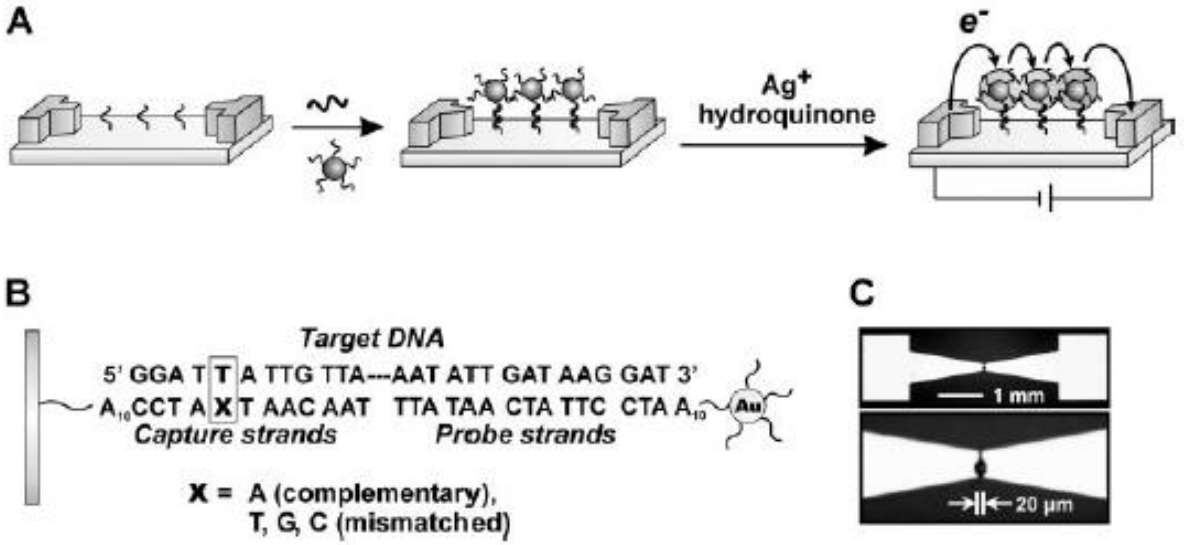

(**A**) Scheme showing concept behind electrical detection of DNA. (**B**) Sequences of capture, target, and probe DNA strands. (**C**) Optical microscope images of the electrodes used in a typical detection experiment. The spot in the electrode gap in the high-magnification image is food dye spotted by a robotic arrayer (GMS 417 Microarrayer, Genetic Microsystems, Woburn, MA).

target DNA was detected at concentrations as low as 500 femtomolar and with a point mutation selectivity factor of ~100,000:1

Park, S. J.; Taton, T. A.; Mirkin, C. A. *Science* **2002**, *295*, 1503-1506.

A nanoplasmonic molecular ruler for measuring nuclease activity and DNA footprinting

G. L. LIU, Y. YIN, S. KUNCHAKARRA, B. MUKHERJEE, D. GERION,
S. D. JETT, D. G. BEAR, J. W. GRAY, A. P. ALIVISATOS, L. P. LEE1, F. F.CHEN
nature nanotechnology **2006**, *1*, 47

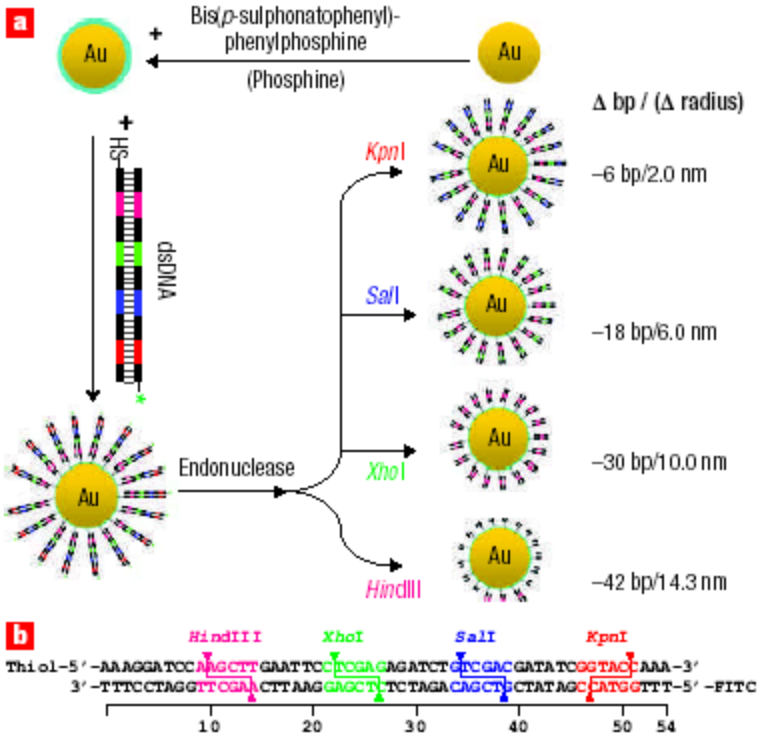

Figure 1. Design of the Au–DNA nanoplasmonic molecular ruler. a, Synthesis process of the Au–DNA nanoconjugate. The 20-nm Au nanoparticle modified with a phosphine surfactant monolayer was enclosed by a layer of synthesized 54-bp dsDNA. A thiol group and the FITC (fluorescein isothiocyanate) fluorophore (as indicated by green star) were synthesized at each end of the dsDNA, respectively. Through the thiol–Au chemistry, the dsDNA was tethered onto the Au nanoparticles. b, The dsDNA contains endonuclease incision sites positioned at 12, 24, 36 and 48 bp from the Au-nanoparticle-tethered end. The fluorescent labelling (FITC) is only for further confirmation of the nuclease reactions, and is not necessary for plasmon resonance measurements.

Gold nanoparticles-based protease assay

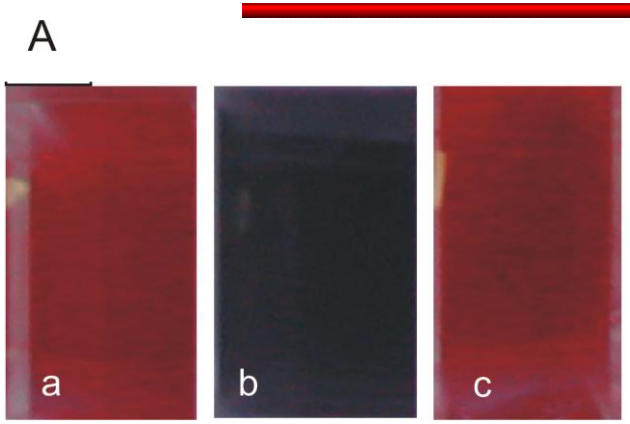

Detection of: **Thrombin and**
Lethal factor of Bacillus Antracis

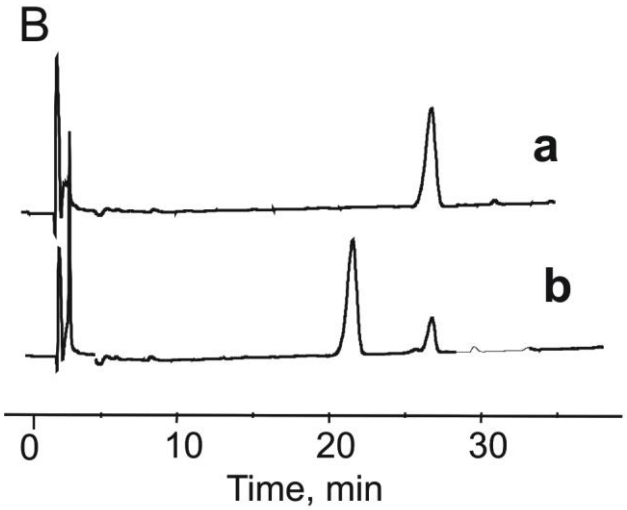

Ac-Cys(S-Ac)-Gly-DPhe-Pro-LArg-Gly-Cys(S-Ac)-OH, 1.

Ac-Cys(S-Ac)-Leu-Arg-Arg-Arg-Arg-Val-Tyr-Pro-Tyr-Pro- nor-Leu-Glu-Leu-Cys(S-Ac)-OH, 2.

Figure 1. A. Color of the gold colloids: (a) untreated solution; (b) 5 min after the addition of **1** ([**1**]=62 nM); (c) 5 min after the addition of **1** ([**1**]final=62 nM) incubated for 90 min with thrombin ([thrombin]=35 nM, [**1**]=62 μM). **B**. RP-HPLC chromatogram of the original peptide **1** (upper trace, a) and after exposition for 60 min to thrombin (lower trace, b). Conditions: [**1**]final=62 μM, [thrombin]= 30 nM, pH=8, 25° C. The peak at 21.5 min corresponds to the fragment Ac-Cys(S-Ac)-Gly-(D)Phe-Pro-Arg-OH.

C. Guarise, L. Pasquato, V. De Filippis, P. Scrimin, *Proc. Natl. Acad. Sci. U.S.A.*, **2006**, *103*, 3978-3982

Gold nanoparticles-based protease assay

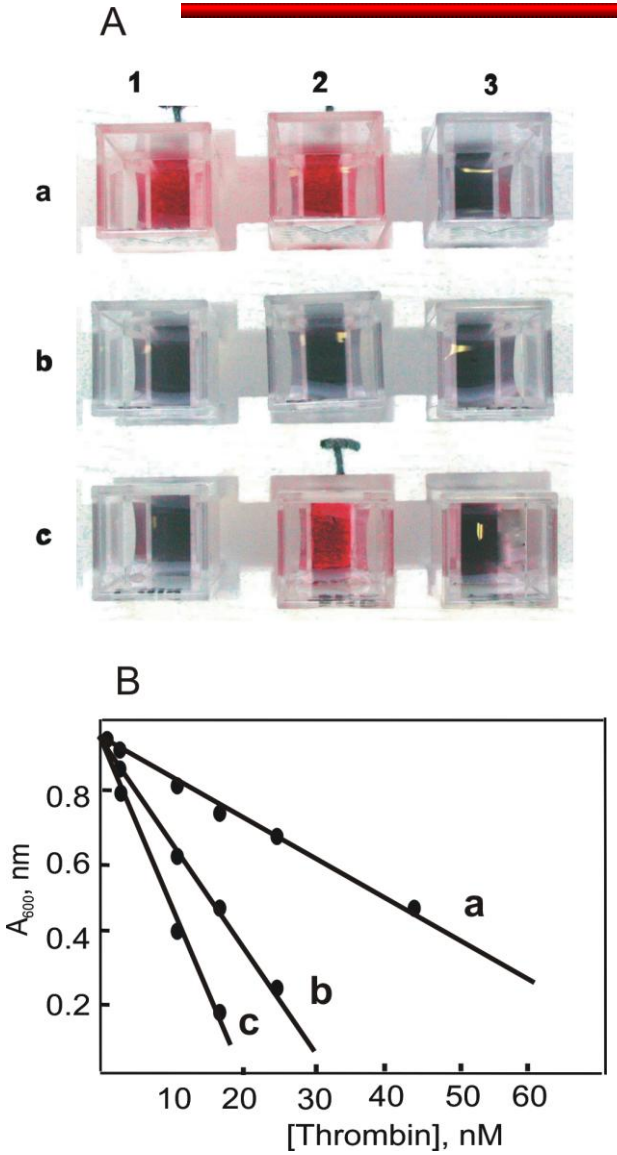

Fig. 3. Thrombin assay. (*A*) Colorimetric test for the presence of thrombin. Each cuvette contained the following enzymes: *a1*, chymotrypsin, plasmin, factor Xa, and thrombin; *a2*, chymotrypsin and thrombin; *a3*, chymotrypsin, plasmin, and factor Xa; *b1*, factor Xa and chymotrypsin; *b2*, chymotrypsin; *b3*, factor Xa; *c1*, none; *c2*, thrombin; *c3*, plasmin. (*B*) Absorbance at 600nmof the gold colloid solution after addition of a solution of peptide **1** ([**1**]final62 nM) exposed to different concentrations of thrombin for 30 min (line a), 60 min (line b), and 90 min (line c) at pH 8 and 25˚ C.

C. Guarise, L. Pasquato, V. De Filippis, P. Scrimin, *Proc. Natl. Acad. Sci. U.S.A.*, **2006**, *103*, 3978-3982

Gold nanoparticles-based protease assay

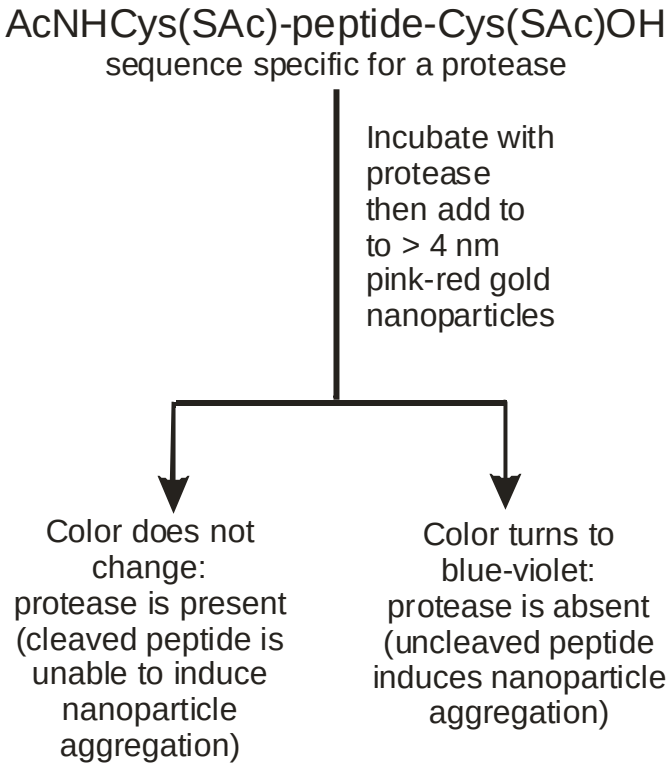

C. Guarise, L. Pasquato, V. De Filippis, P. Scrimin, *Proc. Natl. Acad. Sci. U.S.A.*, **2006**, *103*, 3978-3982

Hybrid Nanoparticle−Liposome Detection of Phospholipase Activity

Daniel Aili†, Morgan Mager†, David Roche and Molly M. Stevens
Nano Letters 2010

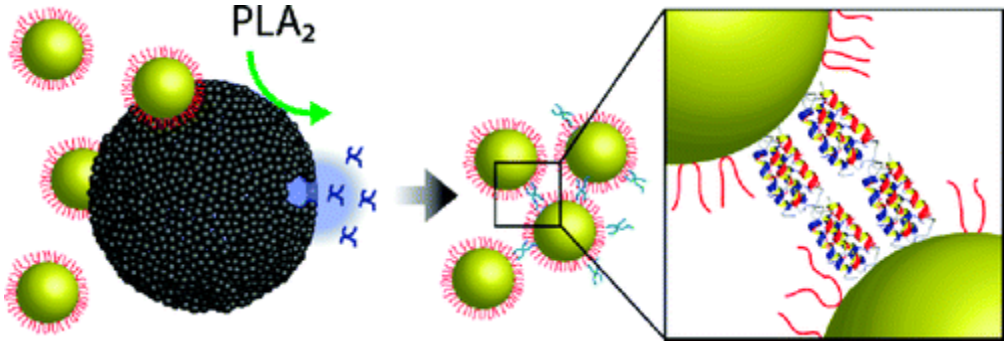

A flexible nanoparticle-based phospholipase (PL) assay is demonstrated in which the enzymatic substrate is decoupled from the nanoparticle surface. Liposomes are loaded with a polypeptide that is designed to heteroassociate with a second polypeptide immobilized on gold nanoparticles. Release of this polypeptide from the liposomes, triggered by PL, induces a folding-dependent nanoparticle bridging aggregation. The colorimetric response from this aggregation enables straightforward and continuous detection of PL in the picomolar range. The speed, specificity, and flexibility of this assay make it appropriate for a range of applications, from point of care diagnostics to high-throughput pharmaceutical screening.

Detection and identification of proteins using nanoparticle–fluorescent polymer ‘chemical nose’ sensors

C.-C. YOU, O. R. MIRANDA, B. GIDER1, P. S. GHOSH, I.-B. KIM,
B. ERDOGAN1, S. A. KROVI, U. H. F. BUNZ, VINCENT M. ROTELLO
nature nanotechnology VOL 2 |MAY 2007 , page 318

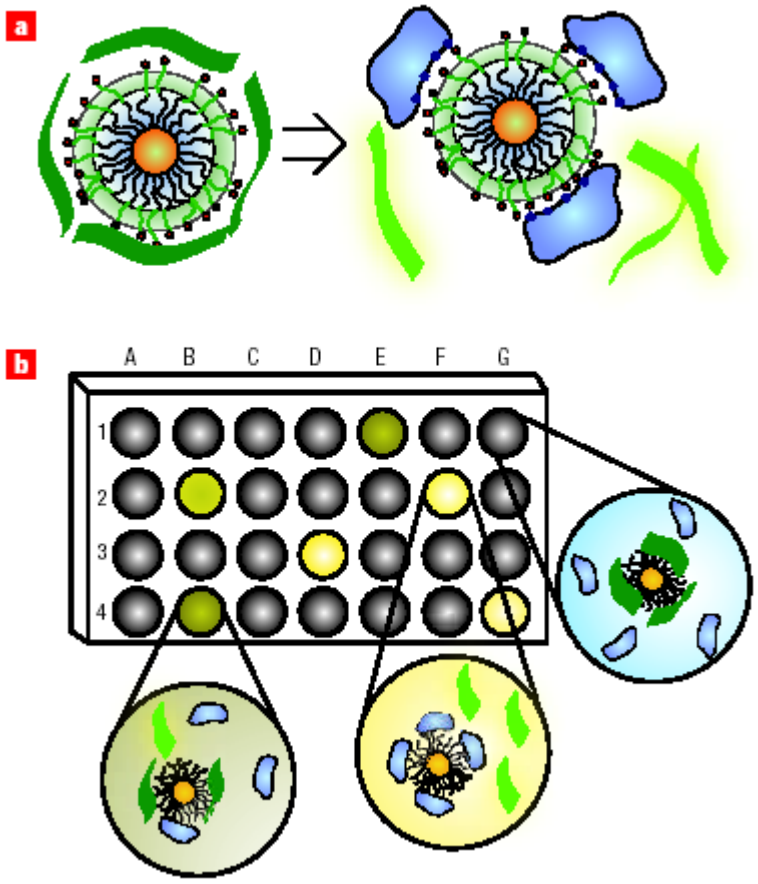

Figure 1 Fluorophore displacement protein sensor array. a, Displacement of quenched fluorescent polymer (dark green strips, fluorescence off; light green strips, fluorescence on) by protein analyte (in blue) with concomitant restoration of fluorescence. The particle monolayers feature a hydrophobic core for stability, an oligo(ethylene glycol) layer for biocompatibility, and surface charged residues for interaction with proteins. **b**, Fluorescence pattern generation through differential release of fluorescent polymers from gold nanoparticles. The wells on the microplate contain different nanoparticle–polymer conjugates, and the addition of protein analytes produces a fingerprint for a given protein.

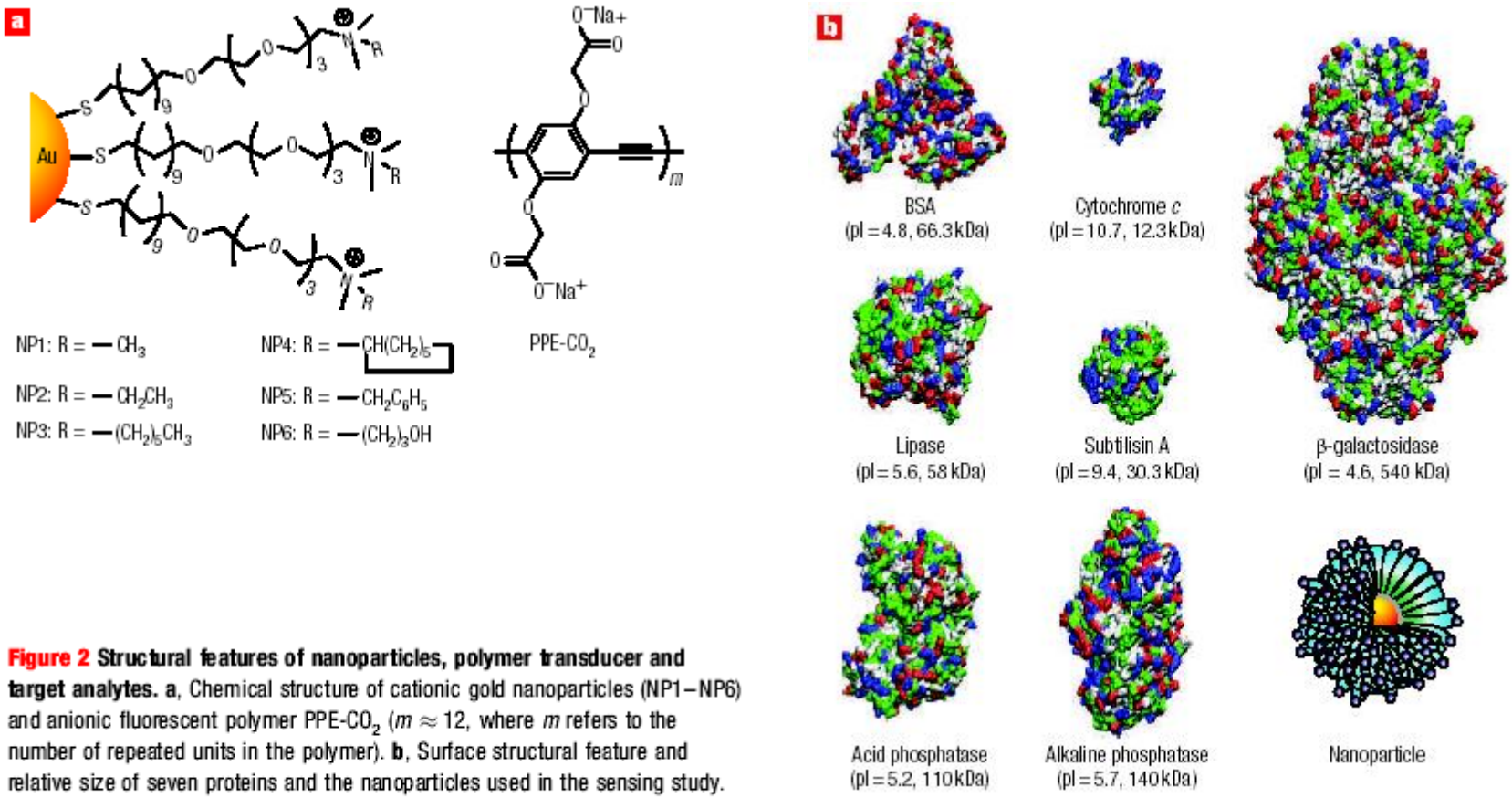

Figure 2 Structural features of nanoparticles, polymer transducer and target analytes. **a**, Chemical structure of cationic gold nanoparticles (NP1–NP6) and anionic fluorescent polymer PPE-CO_2 ($m \approx 12$, where m refers to the number of repeated units in the polymer). **b**, Surface structural feature and relative size of seven proteins and the nanoparticles used in the sensing study. Colour scheme for the proteins: nonpolar residues (grey), basic residues (blue), acidic residues (red) and polar residues (green).

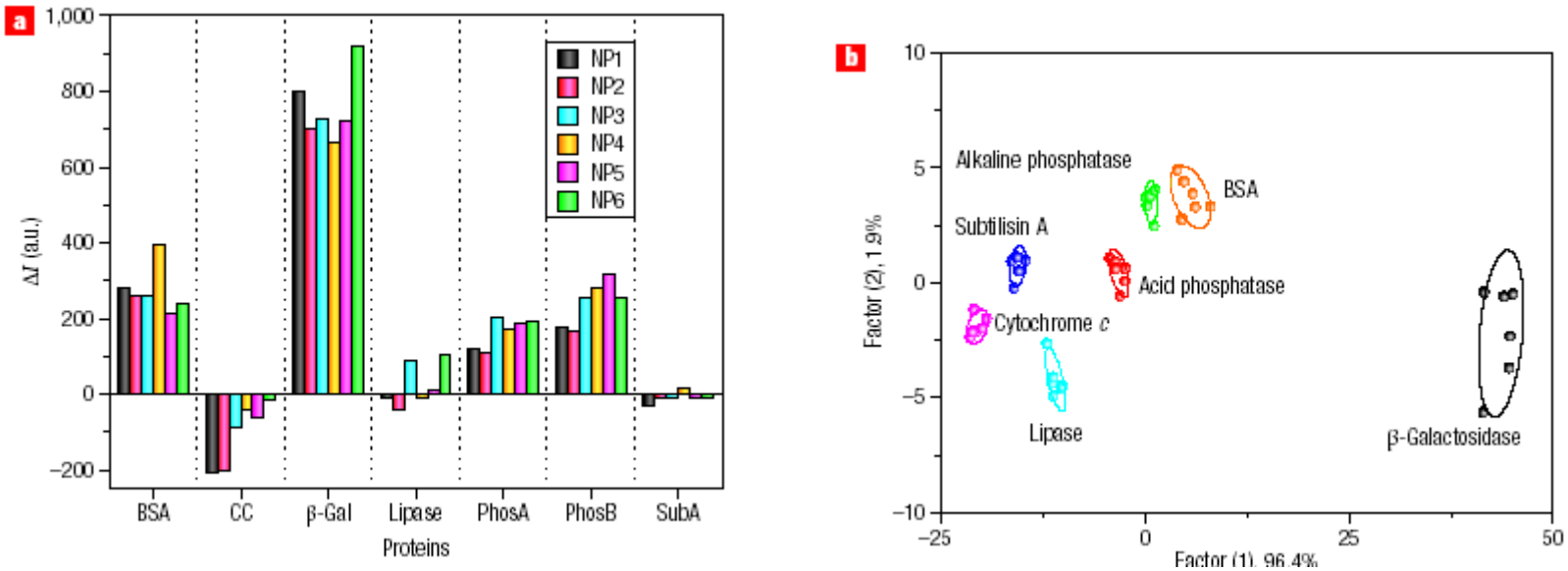

Figure 4 Array-based sensing of protein analytes at 5 μM. a, Fluorescence response (ΔI) patterns of the NP–PPE sensor array (NP1–NP6) against various proteins (CC, cytochrome *c*; β-Gal, β-galactosidase; PhosA, acid phosphatase; PhosB, alkaline phosphatase; SubA, subtilisin A). Each value is an average of six parallel measurements. **b**, Canonical score plot for the first two factors of simplified fluorescence response patterns obtained with NP–PPE assembly arrays against 5 μM proteins. The canonical scores were calculated by LDA for the identification of seven proteins. The 95% confidence ellipses for the individual proteins are also shown.

LDA = linear discriminant analysis

Gold nanostars

Plasmonic nanosensors with inverse sensitivity by means of enzyme-guided crystal growth

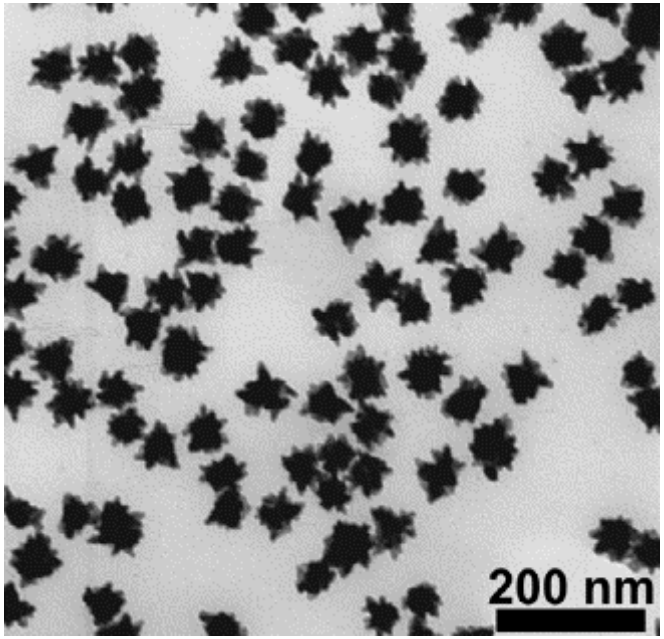

TEM image of Au nanostars synthesized through reduction of $HAuCl_4$ in a PVP/DMF mixture, in the presence of preformed Au seeds, using 10 mM PVP (Mw = 24 000).

L. Rodríguez-Lorenzo, R.de la Rica, R. A. Álvarez-Puebla, L. M. Liz-Marzán M. M. Stevens *Nature Mater.* ***2012****, 11, 604.*

Gold nanostars

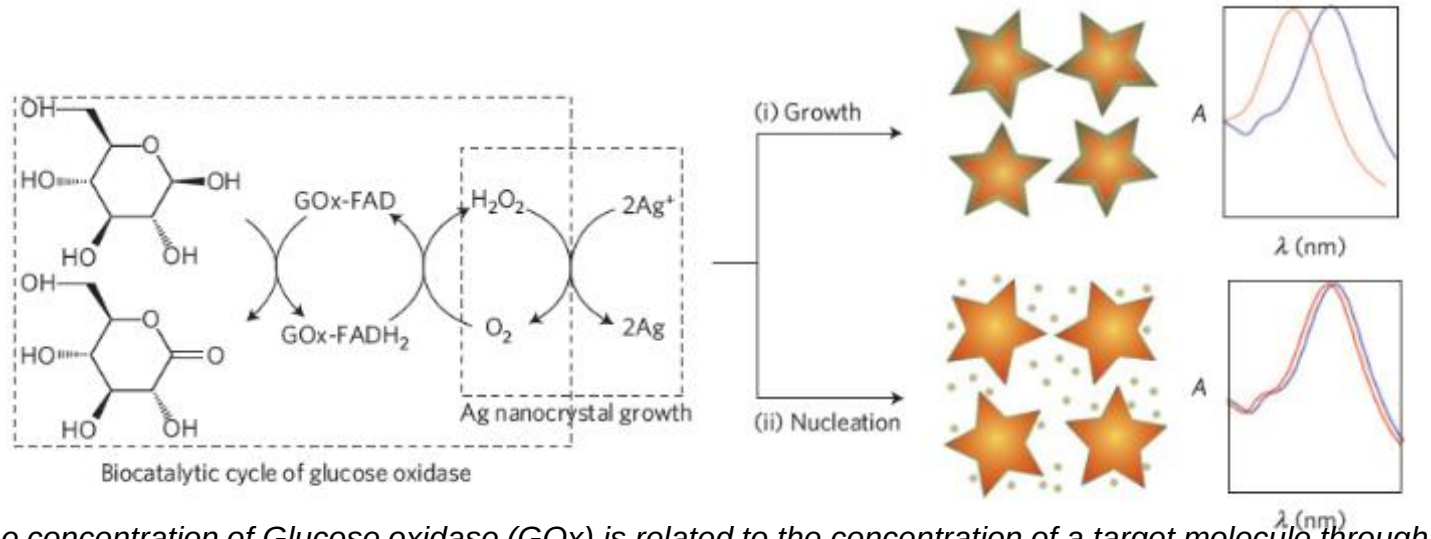

When the concentration of Glucose oxidase (GOx) is related to the concentration of a target molecule through immunoassay, this signal-generation step induces inverse sensitivity because condition (i) is fulfilled at low concentrations of analyte. FAD and FADH2 are the oxidized and reduced forms of flavin adenine dinucleotide.

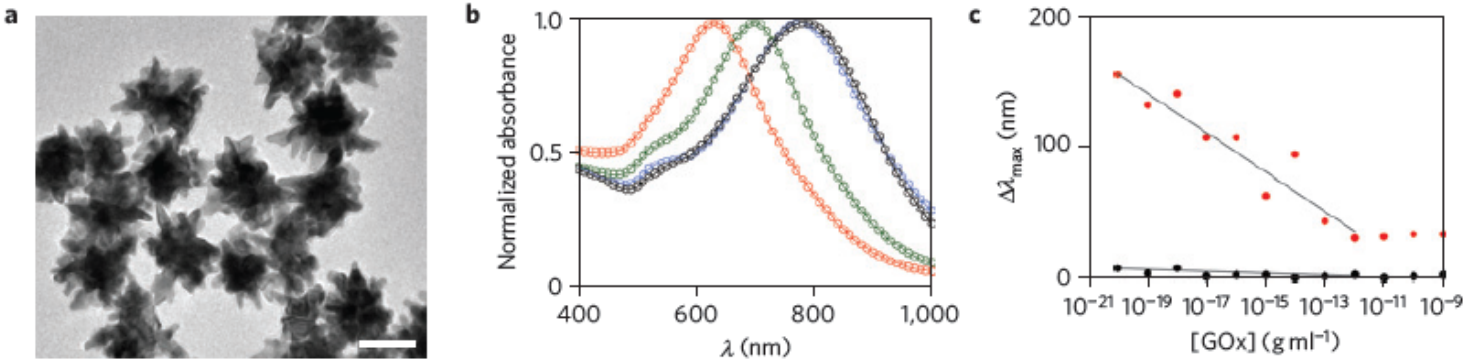

Figure 2 | Inverse sensitivity in plasmonic nanosensors. a, TEM image of gold nanostars (scale bar, 50 nm). **b**, Visible/near-infrared spectra of the nanosensors (black), modified with 10^{-14} g ml^{-1} GOx (green), 10^{-20} g ml^{-1} GOx (red) and without GOx (blue) after the signal-generation step. **c**, Blueshift of the LSPR absorbance band ($\Delta\lambda$max) as a function of the concentration of GOx in the immobilization solution when the signal-generation step is performed in the absence (black) or in the presence (red) of the enzyme-substrate glucose (semilogarithmic scale). The spectral shift was calculated with respect to the control experiment in the absence of GOx (blue curve in **b**).

Organization of simple sub-units in complex structures

…the tools available in supramolecular chemistry

multivalency

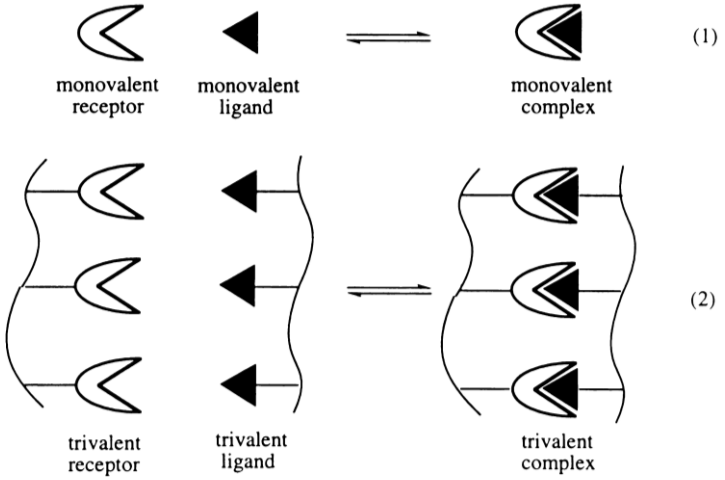

recognition

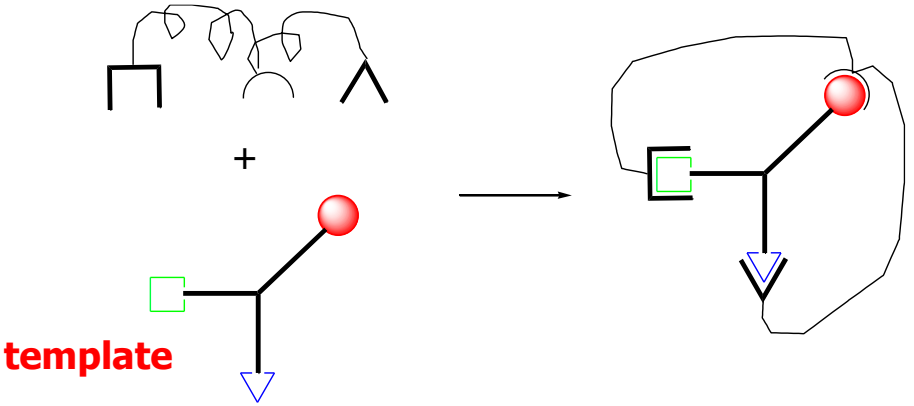

Interactions between groups spatially closed

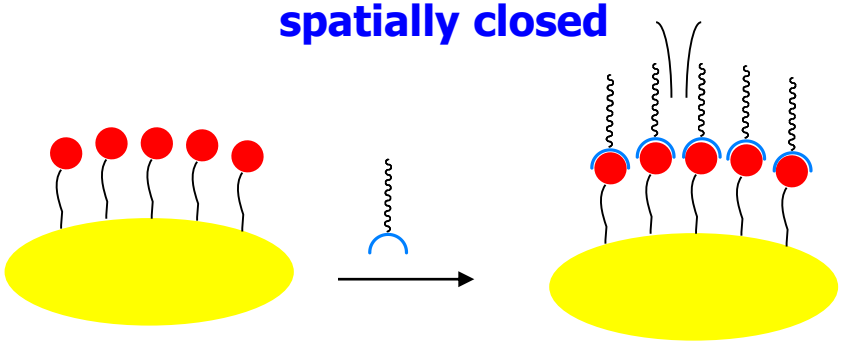

CATALYSIS

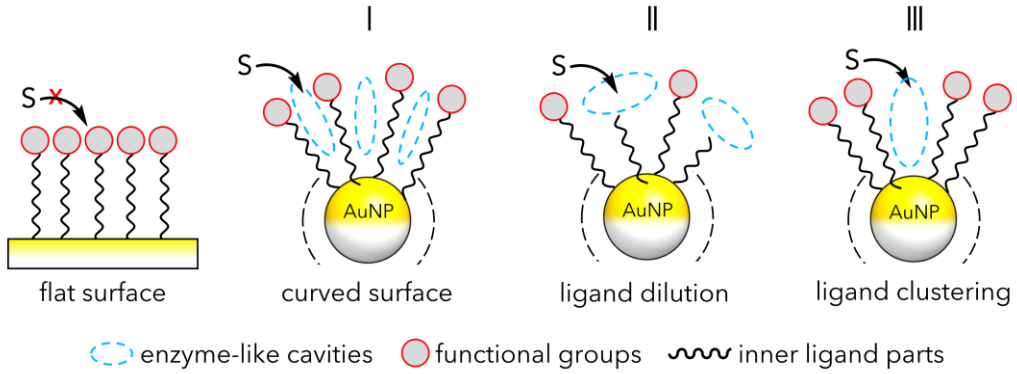

Difference between SAMs on a flat and a curved surface. On a curved surface, the formation of interligand voids within the organic monolayer - accessible to external molecules or substrates (S) - is possible (I) thanks to the increased surface curvature. The size and shape of these pockets can further be modulated by dilution of functional ligands with background ones (II) and/or through ligand clustering (III) leading to self-organized nanoreceptors.

CATALYSIS

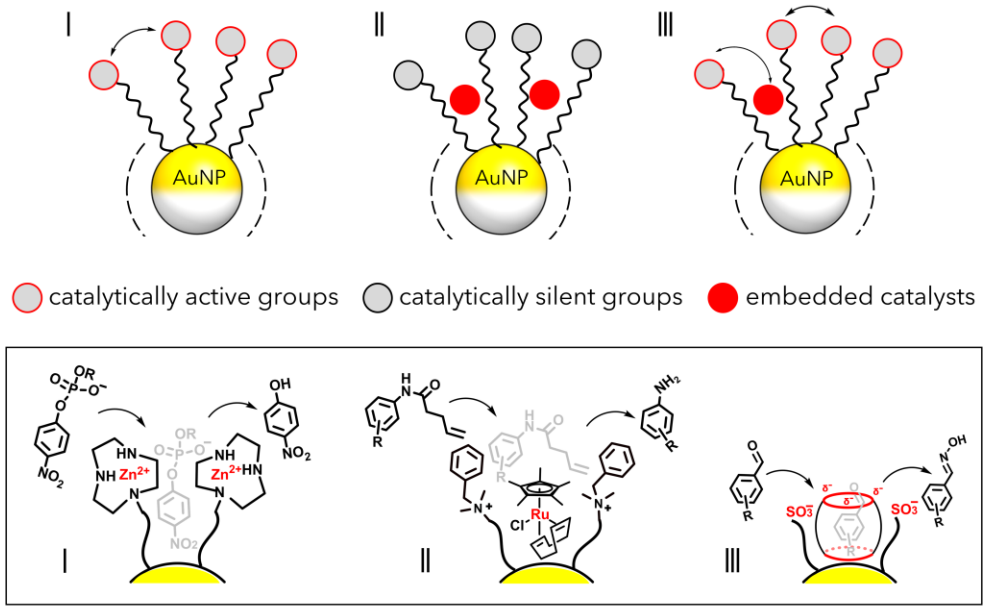

General approaches to nanozyme design: (I) through interactions between proximal functional groups; (II) via embedment of a molecular catalyst within a catalytically inactive monolayer; (III) through embedment and interaction of a molecular catalyst with a catalytically active monolayer.

catalytic activity of MPC-C12-TEG-C12-P2-H

HS-C11-CO-Leu-Gly-Tyr-Lys-Ala-His-Phe-Ala-Gly-Arg-Gly-Arg-OH

P2 =

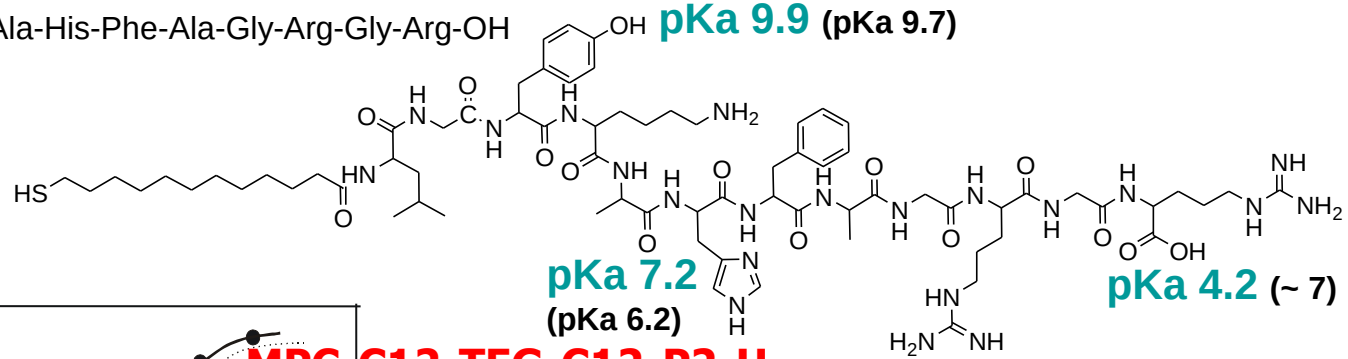

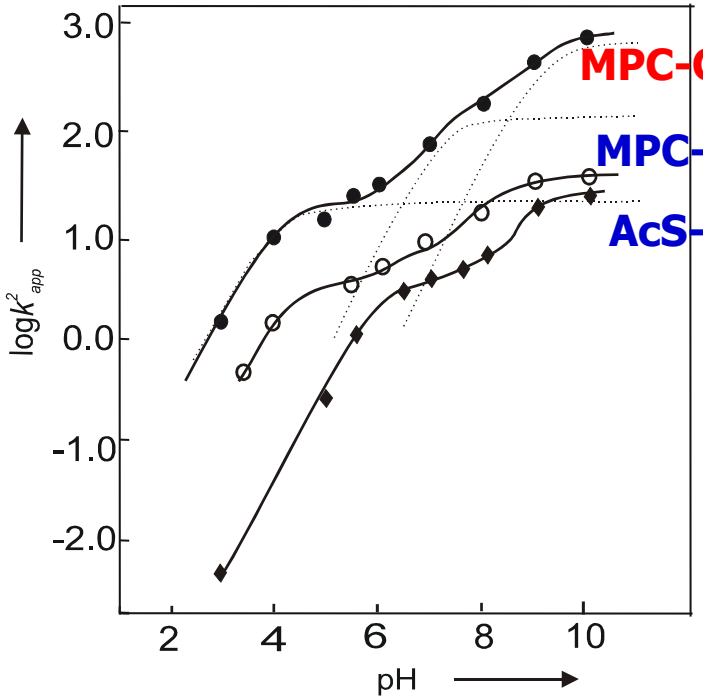

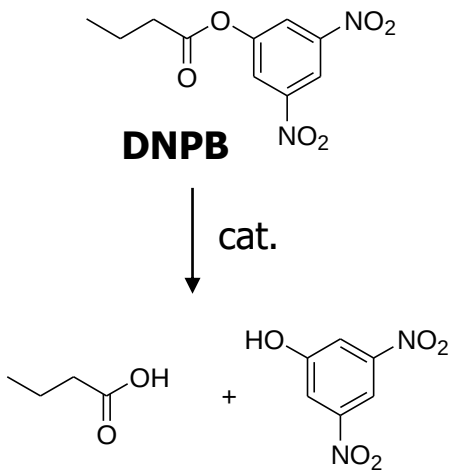

3000-fold rate acceleration (over Ac-C12-HFOH)
500-fold acceleration (over AcS-C12-P2-H)

Log of the apparent second order rate constant against pH for the hydrolysis of DNPB catalyzed by nanoparticles Au-PEP (●) nanoparticles Au-**2** (○), and *S*-acetylated peptide **1** (♦). The solid lines represent the best fits of functions describing the dissociation of residues involved in catalysis with p*K*a values of 4.2, 7.2 and 9.9, in the case of Au-PEP, 4.2 and 8.1 for Au-**2**, and 6.1 and 9.2 for *S*-acetylated **1**. The dotted lines represent the calculated contribution of each species to the solid curve for Au-PEP. Conditions: [catalyst]=4.0×10^{-5} M, [buffer]=10-20 mM, 25° C.

Pengo, P.; Baltzer, L.; Pasquato, L.; Scrimin, P. *Angew. Chem. Int. Ed.* **2007**, *46*, 400-404.

catalytic activity of MPC-C8-TEG-C12-P2-H

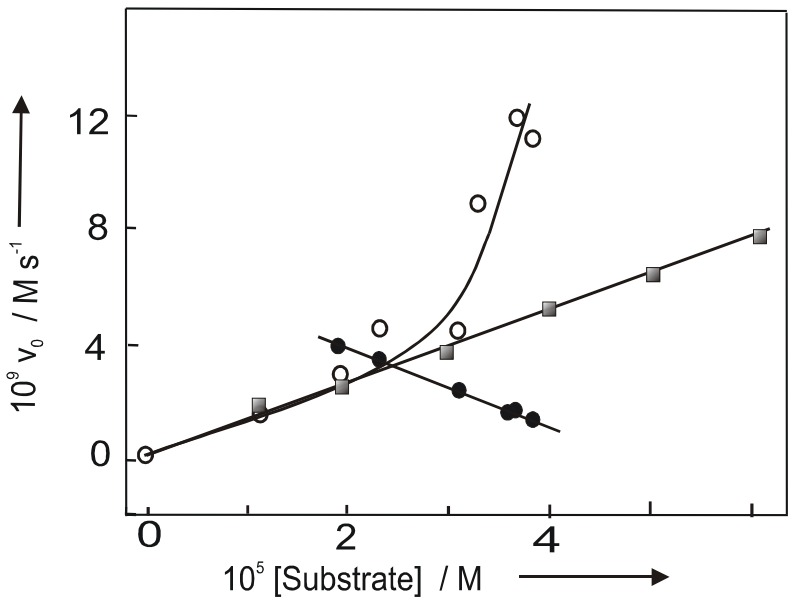

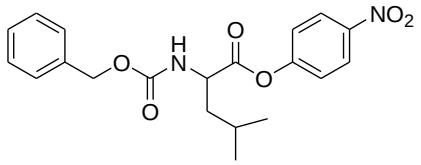

Z-(L)-Leu-ONp

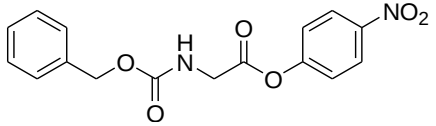

Z-Gly-ONp

DNPB behaves as Z-Gly-ONp

Figure 2. Dependence of the initial rate (M s^{-1}) of intermediate formation (○) and its hydrolysis (●) with Z-Leu-PNP and that of hydrolysis (■) with Z-Gly-PNP upon substrate concentration. Conditions: [**S-C12-P2-OH**]=1.3×10^{-5} M (bound to Au-PEP), pH 7, 25° C.

$$\text{Cat} + \text{S} \underset{k_-}{\overset{k_+}{\rightleftharpoons}} \text{Cat-S} \xrightarrow{k_{cat}} \text{Cat-S'} + \text{P1} \xrightarrow{k_2} \text{Cat} + \text{P2}$$

serine-proteases like activity

Pengo, P.; Baltzer, L.; Pasquato, L.; Scrimin, P. *Angew. Chem. Int. Ed.* **2007**, *46*, 400-404.

nanomaterials for diagnosis, imaging, and therapy

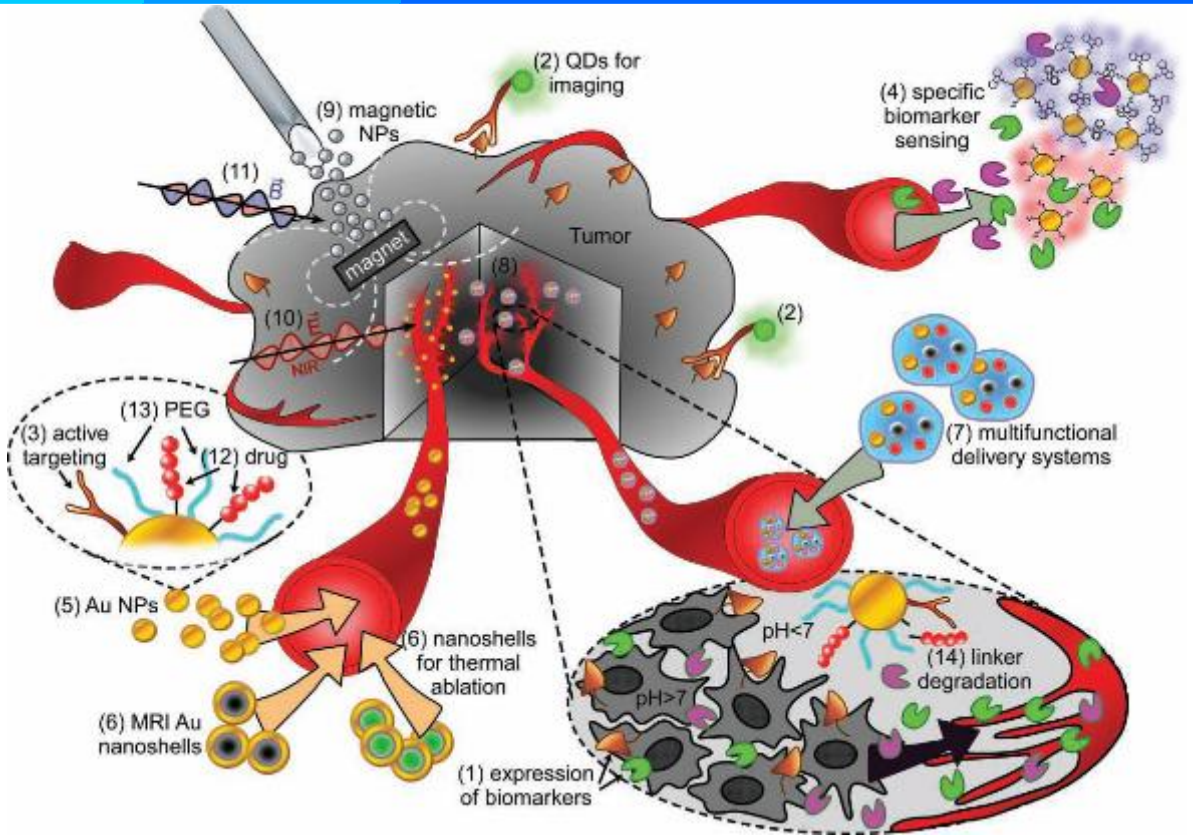

C. Minelli, S. B. Lowe, M. M. Stevens *Small* **2010**, *6*, 2336-2357.

- improved delivery of poorly water-soluble drugs
- targeted delivery of drugs in a cell- or tissue-specific manner
- transcytosis of drugs across tight epithelial and endothelial barriers
- delivery of large macromolecule drugs to intracellular sites of action
- co-delivery of two or more drugs or therapeutic modality for combination therapy
- visualization of sites of drug delivery by combining therapeutic agents with imaging modalities
- real-time read on the *in vivo* efficacy of a therapeutic agent

Multifunctional nanoparticle

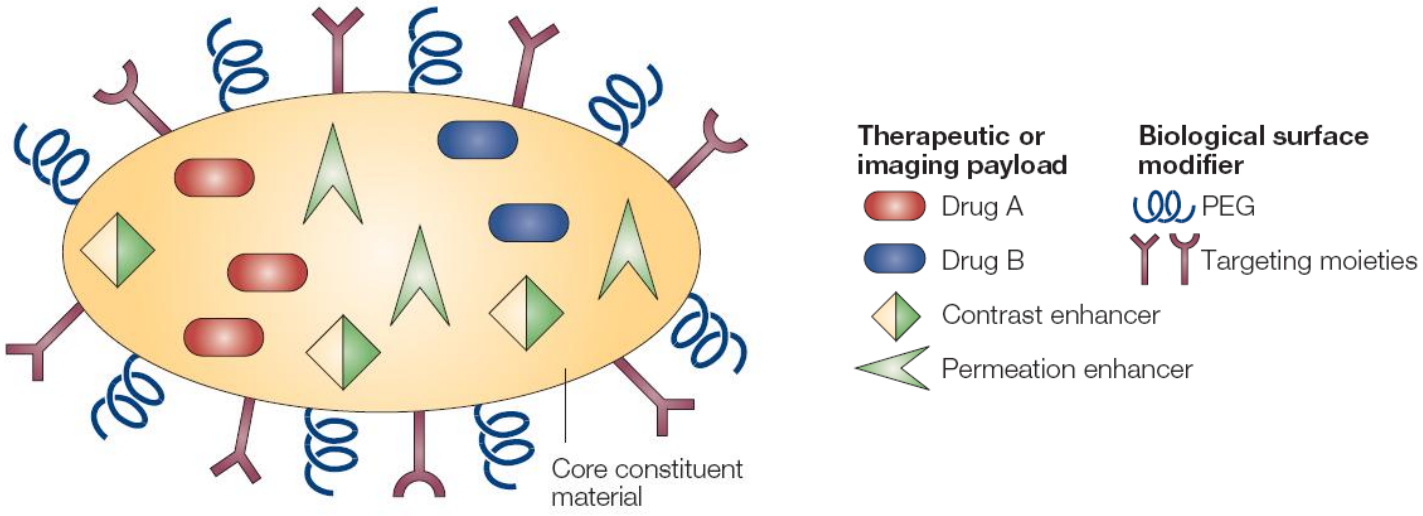

an ideal nanovector should possess:

- the ability to carry one or more therapeutic agents;
- biomolecular targeting through one or more recognition agents;
- imaging elements;
- biobarrier avoidance.

M. Ferrari *Nat. Rev. Cancer* **2005**, *5*, 161-171.

why gold nanoparticles?

Gold NPs have generated significant interest in various biomedical applications

DETECTION
DIAGNOSIS
THERAPY

- Au NPs of many different sizes (1-150 nm) can be fabricated in a controlled fashion with control over size dispersity and shape.

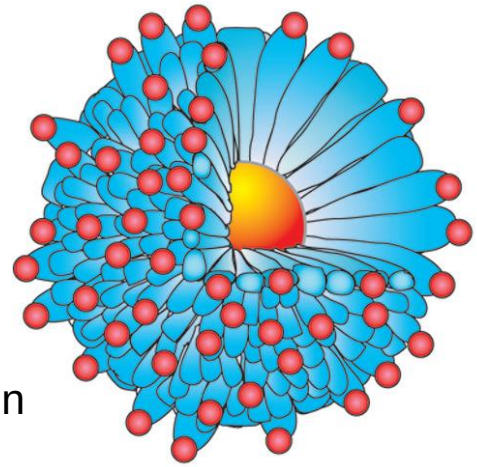

- AuNPs have high surface-area-to-volume ratios, and as a result, a high density of ligands can be appended for targeting and/or drug-delivery.
- Functional diversity can be readly achieved by creation of a multifunctional monolayer.
- The gold core is essentially inert, non toxic, biocompatible making it an ideal nanovector.

photothermal therapy

travel as far through living tissue as a magnetic field can. "We wanted something that

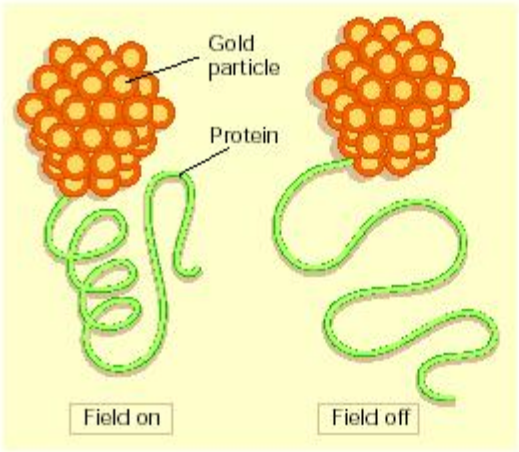

Kimberly Hamad-Schifferli (right) hopes to control proteins by attaching tiny gold particles to them — in a radio field the particle heats up, altering the protein's structure and inactivating it.

'nano' word is over-used and over-hyped," says John Ryan, director of the Nanobiotech-

paced activities of daily life in the cell. And for those in the nanosystems alliance, nanotechnology is the best way to get a grip on the many fleeting processes involved. Alliance member Leroy Hood, a molecular biologist at the Institute for Systems Biology in Seattle, predicts that nanotechnology will reveal as much new information about the cell as did the automated DNA sequencer — a device that he invented. "The combination of microfluidics and nanotechnology," Hood asserts, "will transform how biologists do everything." ■

Catherine Zandonella is a freelance writer in New York.

1. Melosh, N. A. *et al. Science* **300**, 112–115 (2003).
2. Vo-Dinh, T. *J. Cell. Biochem.* **87**, 154–161 (2002).
3. Klarreich, E. *Nature* **413**, 450–452 (2001).
4. Quintana, A. *et al. Pharm. Res.* **19**, 1310–1316 (2002).
5. Hamad-Schifferli, K., Schwartz, J. J., Santos, A. T., Zhang, S. & Jacobson J. M. *Nature* **415**, 152–155 (2002).

Alliance for NanoSystems Biology

www.nanosysbio.org

Gold NPs in Clinical trials

Phase I and Pharmacokinetic of CYT-6091

L. Tamarkin et al. Clin. Cancer Res. ***2010****, 16, 6139.*

CYT-6091 – which is comprised of recombinant human tumor necrosis factor alpha (rhTNF)
Bound to the surface of PEGylated 27 nm colloidal gold particles
85% complete remission rates are routinely observed.
PEGylation of GNPs
- *avoids immediate uptake by the reticuloendothelial reticulum (RES)*
-Reduces the toxicity of rhTNF
-Allows the nanomedicine to sequester in solid tumors
maximal antitumor responses were achieved at lower doses of drug.

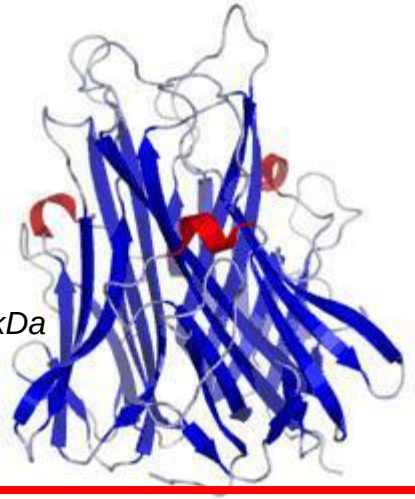

TNF-alpha is a homotrimer with a subunit molecular mass of 17 kDa

Gold NPs in Clinical trials

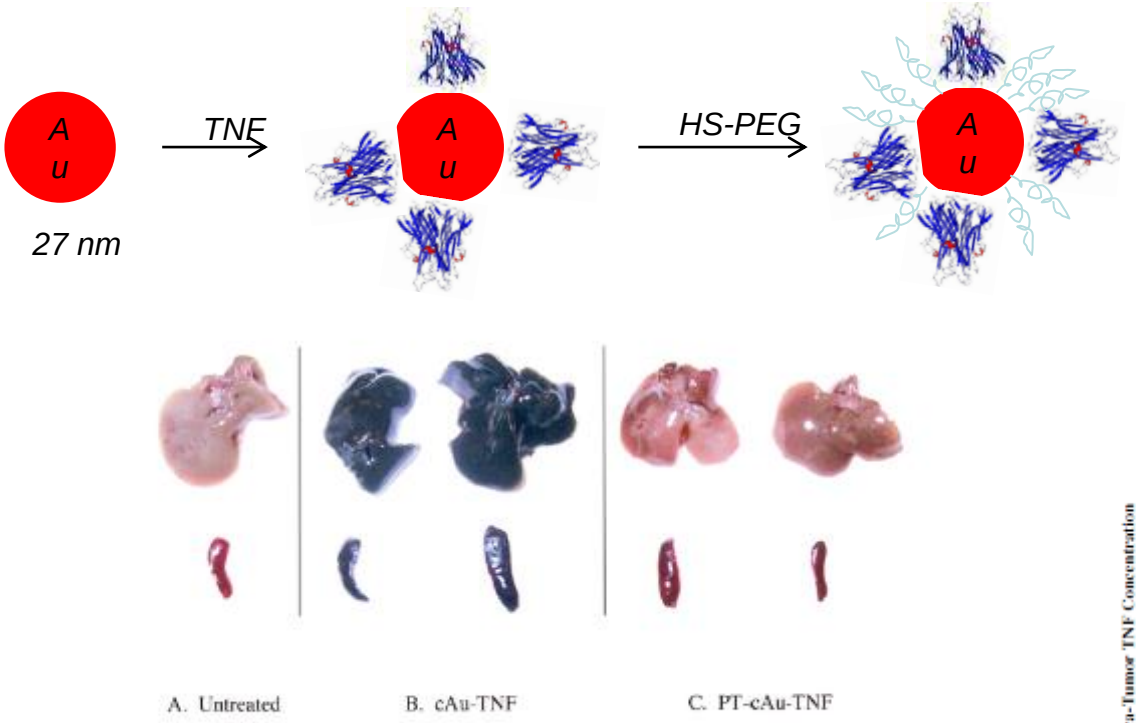

FIG. 2. Hepatic and splenic uptake of the cAu-TNF formulation and the PEG-THIOL cAu-TNF formulation (PT-cAu-TNF) compared to an untreated mouse. Two MC-38 tumor-burdened C57/BL6 mice were injected intravenously with the cAu-TNF vector, and another two tumor-burdened C57/BL6 mice were injected with the PT-cAu-TNF formulation. An untreated mouse and the four treated mice were sacrificed 5 hr after injection of 15 μg of the two different cAu formulations, and all five animals were perfused with heparinized saline. The livers and spleens from these animals were collected and photographed using a digital camera. (a) Liver and spleen from an untreated mouse. (b) Livers and spleens from mice receiving the cAu-TNF vector. (c) Liver and spleen from mice receiving the PT-cAu-TNF vector.

CytImmune is now collaborating with AstraZeneca to add a chemotherapeutic drug to further improve the killing power of CYT-6091.

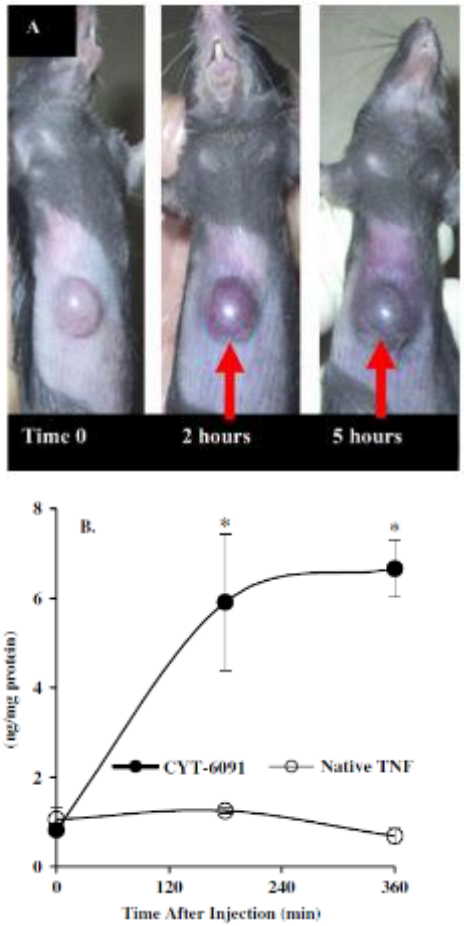

Fig. 3. **A:** Visual documentation of the accumulation of CYT-6091 (red arrows indicate location of the particle drug) in MC-38 tumors. **B:** Sequestration of CYT-6091 and TNF in MC-38 tumors. MC-38 tumor-burdened C57/BL6 mice were injected with 15 μg of either native TNF or CYT-6091. TNF actively accumulates in the MC-38 tumors ($^{*}P<0.05$ vs. native TNF Treatment and the time 0 point for CYT-6091 treatment). Reproduced from Paciotti et al., [2004], with permission of the publisher.

Delivery

drug delivery via 'active' and 'passive' targeting

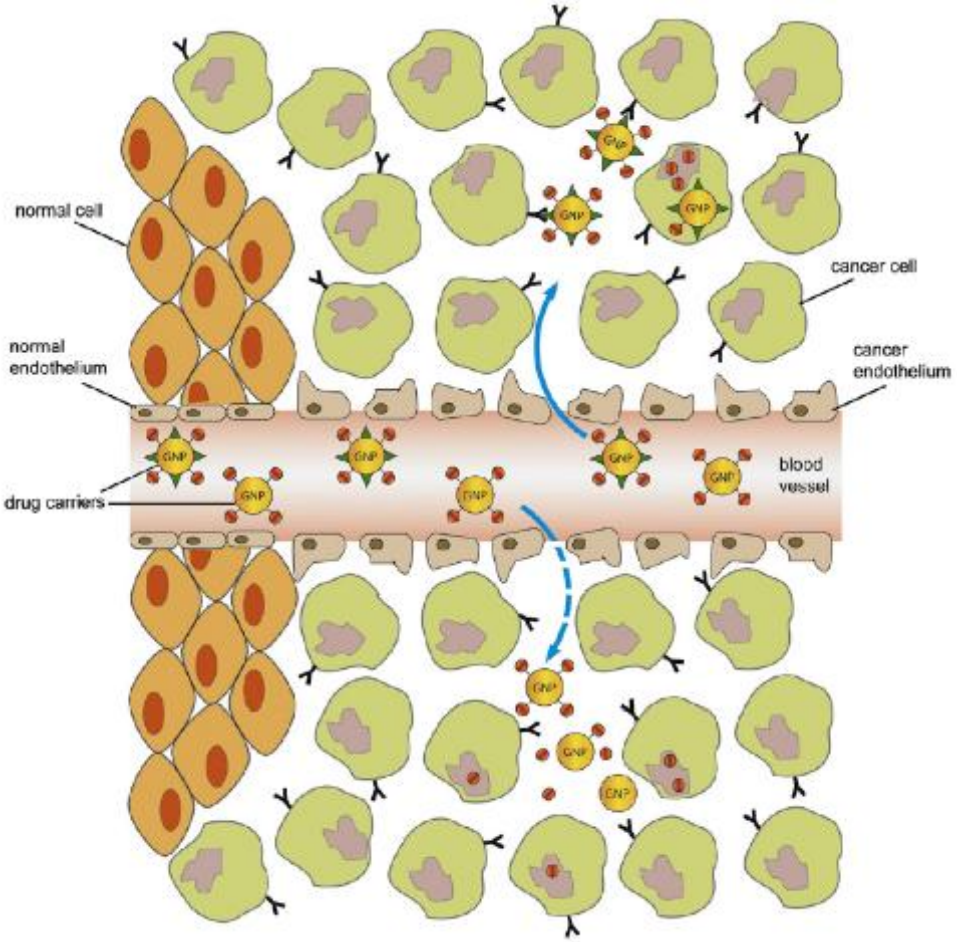

Delivery

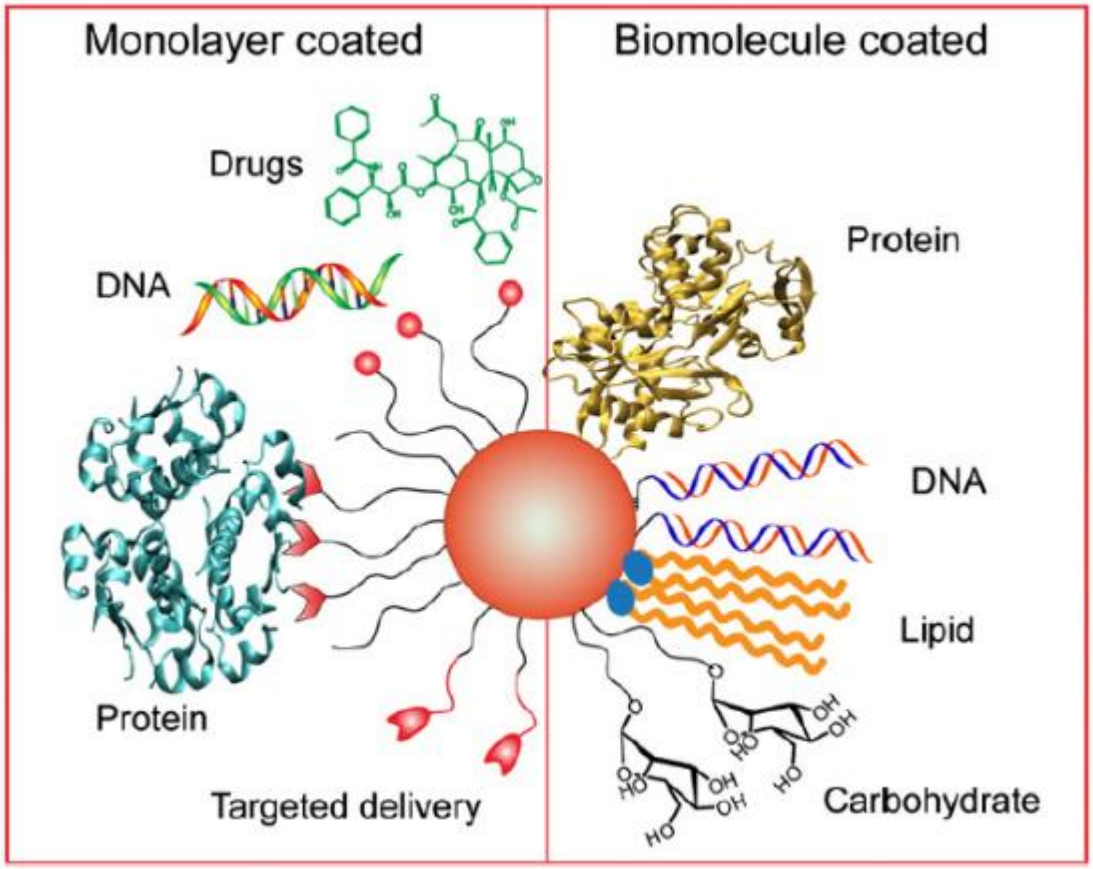

Schematic presentation of the two AuNP surface structures commonly employed in delivery applications.

multimodal drug delivery gold nanoparticles

- Prodrugs can be convalently conjugated to AuNPs via cleavable linkers.
- Hydrophobic drugs can be non-covalently loaded onto AuNPs, allowing conjugation without structural modification of the drug payload.
- The release can be trigger by either internal (e.g. glutathione) or external (e.g. light) stimuli.

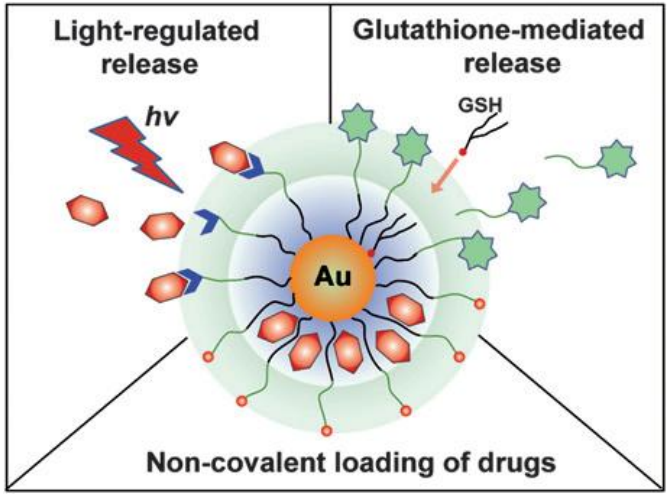

intracellurar GSH concentration 1-10 mM

Encapsulation or conjugation of therapeutic agents with NPs has proven to be a succesful approach

- to improve therapeutic's water solubility
- circulation time in the body
- uptake, in turn reducing drug payloads and associated toxic effects.

Delivery

Au NPs for transfection of DNA

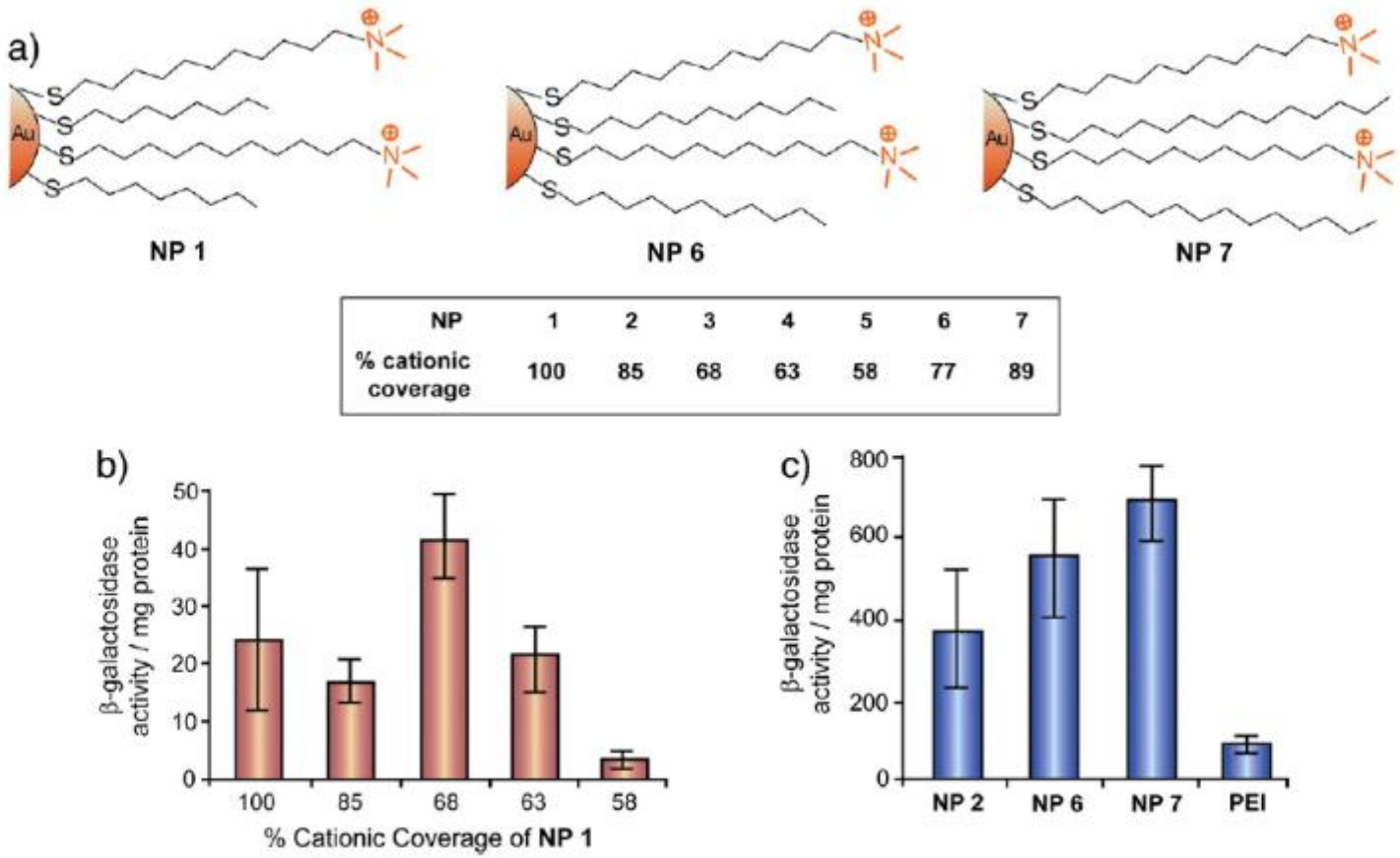

Fig. 3. (a) Structures of cationic NPs varied with amount of cationic ligands (NP 1–5) and alkyl chain length (NP 6–7) used for transfection of DNA. (b) Transfection of β-galactosidase using NP-DNA complexes (at 2200:1 ratio), measured by β-gal activity. (c) Transfection efficiency of NPs 2, 6, 7 (2200:1 NP/DNA ratio) and commercially available PEI (60 kDa).

V. M. Rotello et al. Bioconjug. Chem. 2002, 13, 3–6.

non-covalent loading

Entrapment of Hydrophobic Drugs in Nanoparticle Monolayers with Efficient Release into Cancer Cells

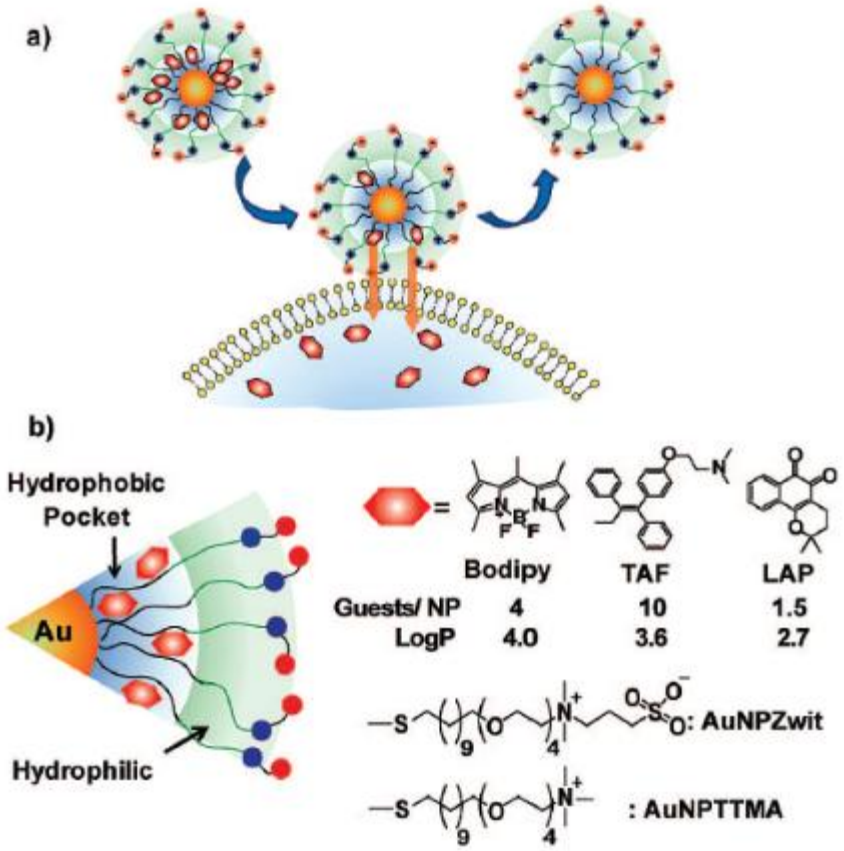

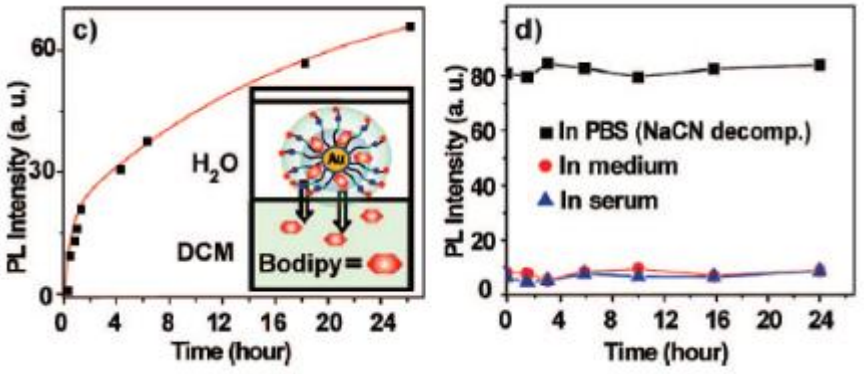

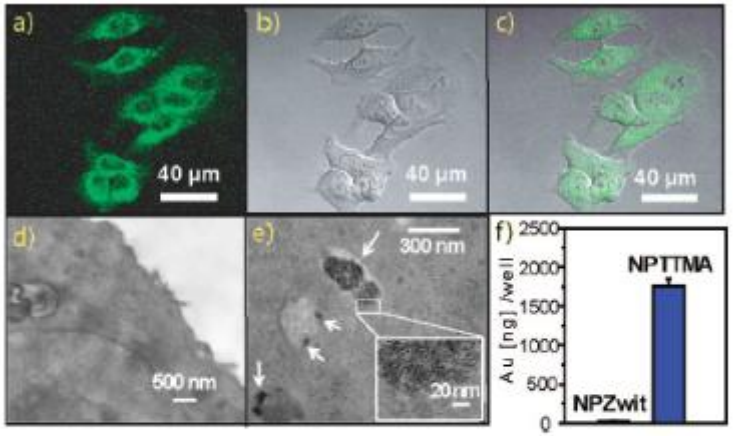

Figure 2. CLSM images of MCF-7 cell treated with **AuNPZwit-Bodipy** for 2 h: (a) green channel, (b) bright field, and (c) overlap. TEM images of fixed cell treated with (d) **AuNPZwit-Bodipy** and (e) **AuNPTTMA** as a positive control. Endosomally trapped AuNPs are marked by arrow. (f) ICP-MS measurement (200 000 cells/well), indicating low cellular uptake of **AuNPZwit** (31 ng/well after 4 h).

V. M. Rotello et al. JACS 2009, 131, 1360.

Covalent binding and light-regulated release

Photoregulated release of anticancer drugs from gold NPs

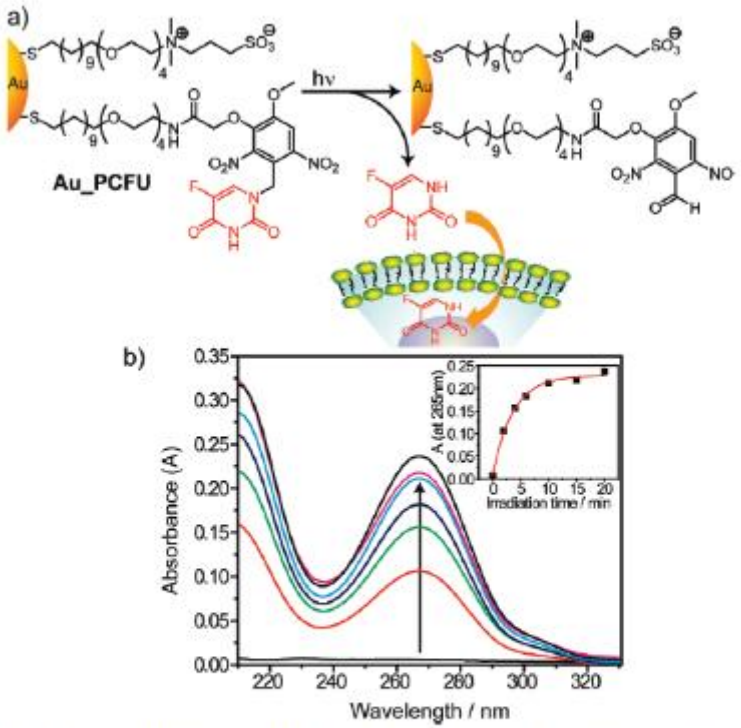

Figure 1. (a) Photochemical reaction of **Au_PCFU** and delivery of payload to cell. (b) Overlaid UV−vis spectral changes showing light dose dependent increase of 5-FU concentration. Inset: The plot of absorbance at 265 nm against irradiation time.

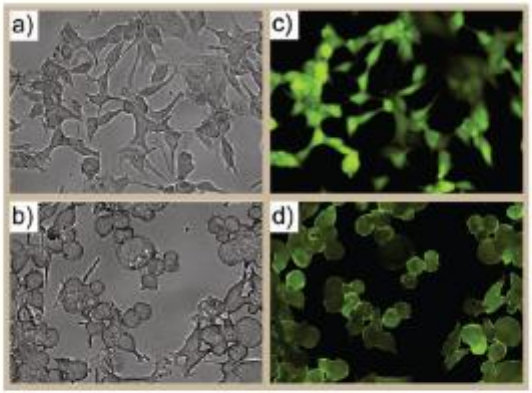

Figure 2. Bright-field and fluorescence-microscopy images of the cells irradiating before treated with **Au_PCFU** (a and c) and irradiating after treated with **Au_PCFU** (b and d).

V. M. Rotello et al. JACS 2009, 131, 5728.

gold nanoparticles for gene delivery

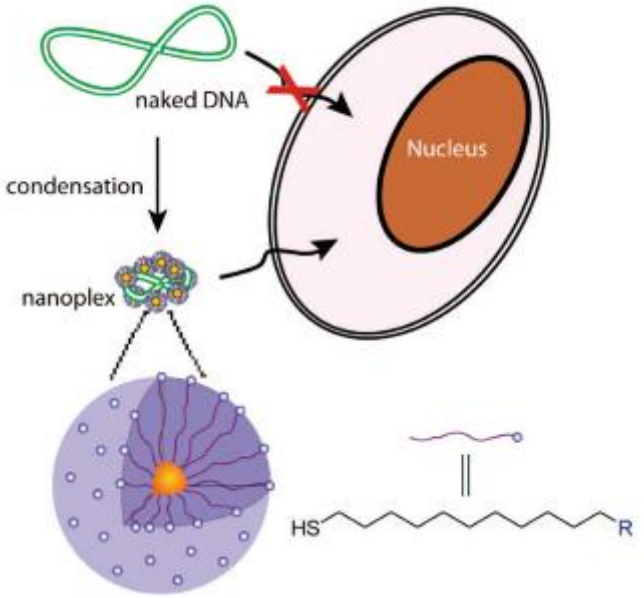

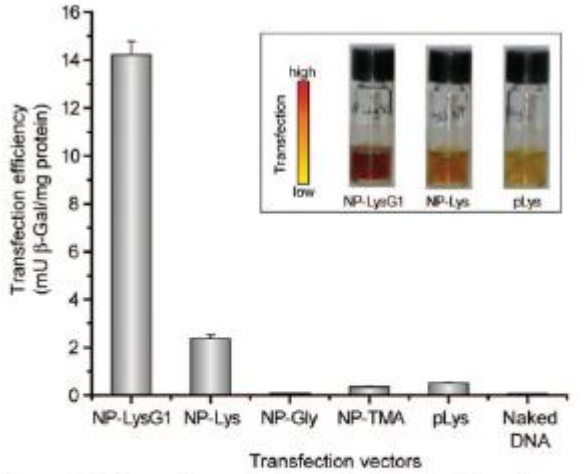

Figure 4. Enhanced transfection using NP−LysG1 and NP−Lys relative to positive controls, NP−TMA, and poly-lysine (pLys). No appreciable enzyme activity was observed in the absence of vectors. Inset shows solution colors during β-Gal activity assay performed after transfection. The color changes from yellow (substrate) to red (product) in the presence of active enzyme.

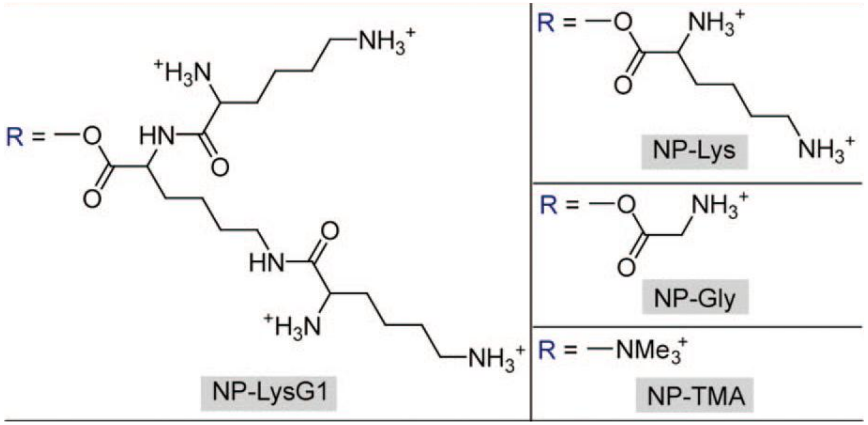

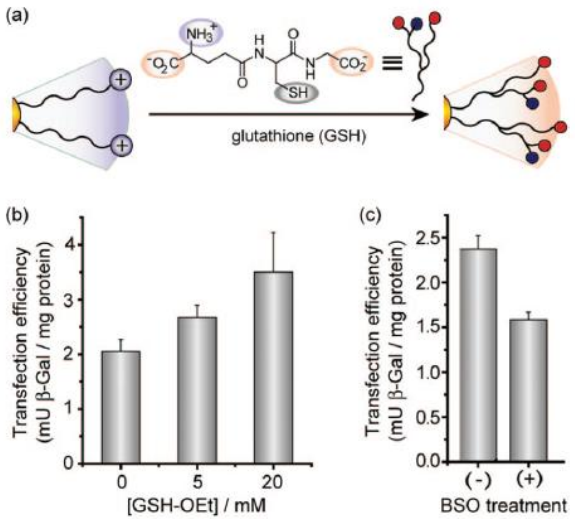

P. S. Ghosh, C.-Kyu Kim, G. Han, N. S. Forbes, V. M. Rotello
ACS Nano **2008**, *2*, 2213-2218.

gold nanocages for drug delivery trigger by light

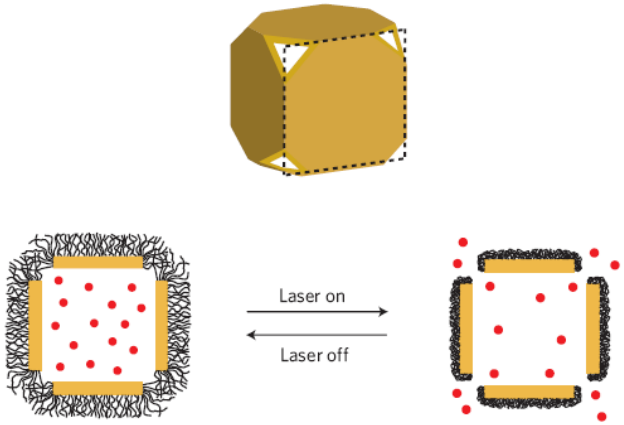

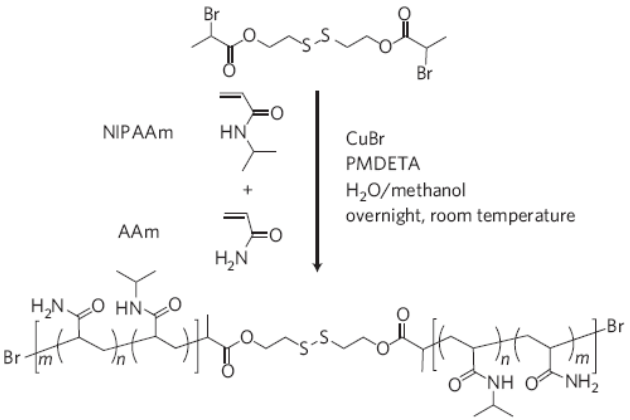

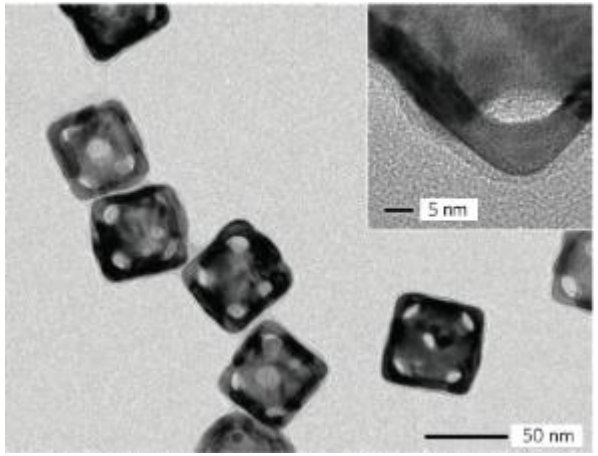

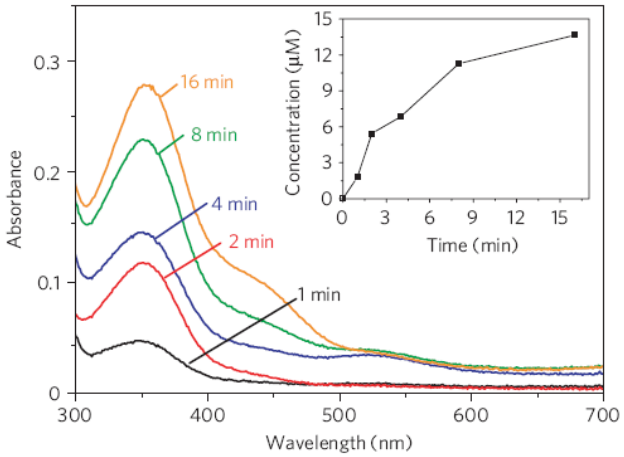

M. S. Yavuz, Y. Cheng, J. Chen, C. M. Cobley, Q. Zhang, M. Rycenga, J. Xie, C. Kim, K. H. Song, A. G. Schwartz, L. V..Wang, Y. Xia *Nat. Mater.* **2009**, *8*, 935-939.

Immobilization of Gold Nanoparticles on Living Cell Membranes upon Controlled Lipid Binding

Haojin Ba, Jessica Rodrı´guez-Ferna´ndez,* Fernando D. Stefani,† and Jochen Feldmann

Nano Lett. **2010,** *10*, 3006–3012

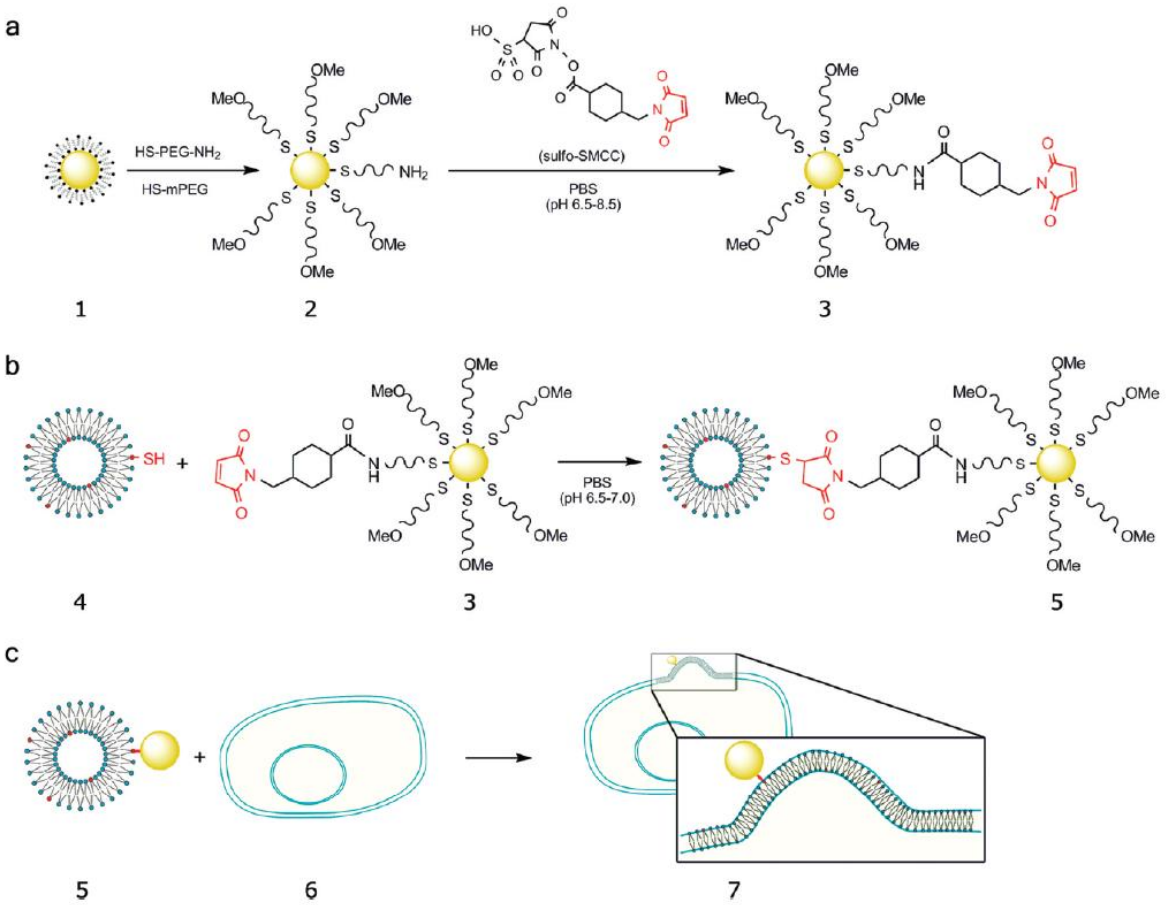

FIGURE 1. Sketch depicting the general strategy for surface modification, lipid binding, and final cell membrane incorporation of Au nanoparticles. (a) PEGylation and subsequent maleimide functionalization of CTAB-capped Au nanospheres. (b) Conjugation of the maleimide-functionalized nanoparticles to liposomes containing a thiolated lipid (PTE−SH). (c) Fusion of the Au@mal-tagged liposomes with the cell membrane of Jurkat cells. The numbers refer to Au@CTAB (1), Au@mPEG−SH/HS−PEG−NH_2 (2), and Au@mal (3) nanoparticles, respectively; small liposomes containing PTE−SH (4), Au@mal bound to PTE−SH in liposomes (5), living (Jurkat) cell (6), and Au@mal tagged to PTE−SH in the cell membrane, after liposome/membrane fusogenesis (7).

Au-NPs as catalysts

heterogeneus catalysis

oxidation reactions

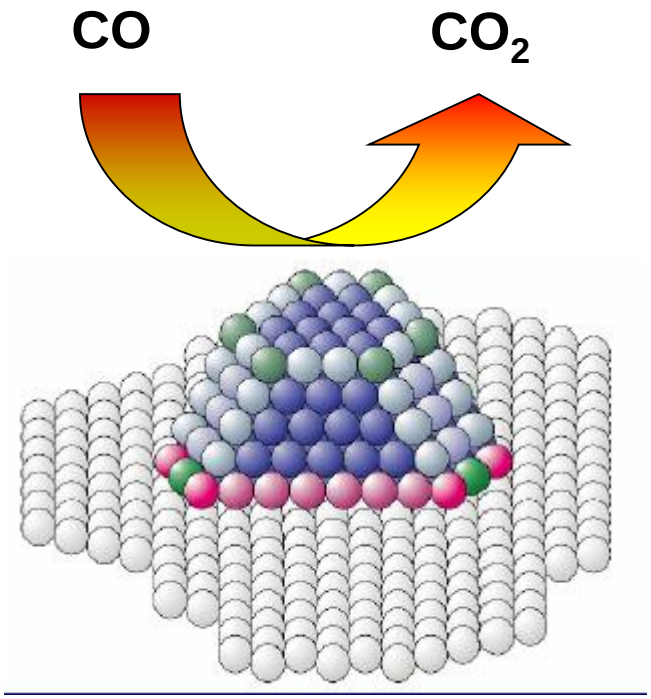

Au-NPs as catalysts

oxidation of CO for H_2 purification

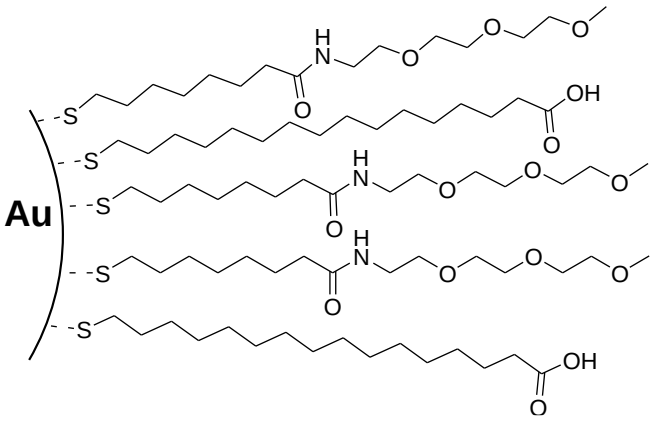

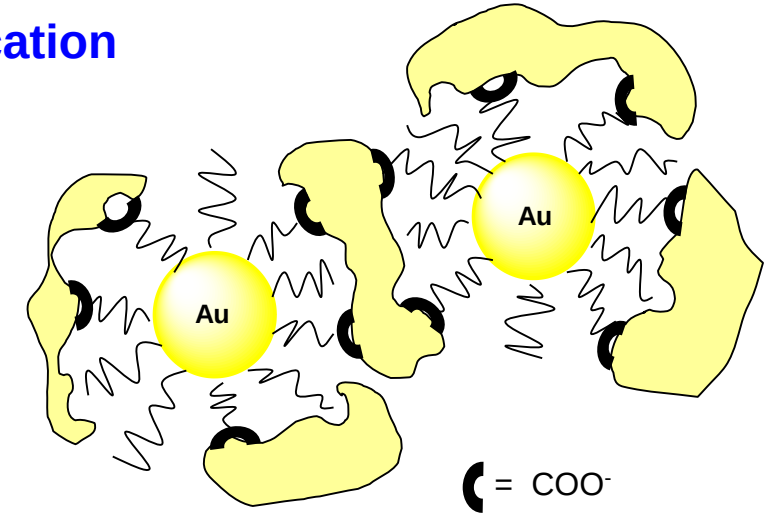

PROX conditions: CO (1%) + O_2 (1%) + H_2 (47.5%) + CO_2 (17.5%) + H_2O (5%)

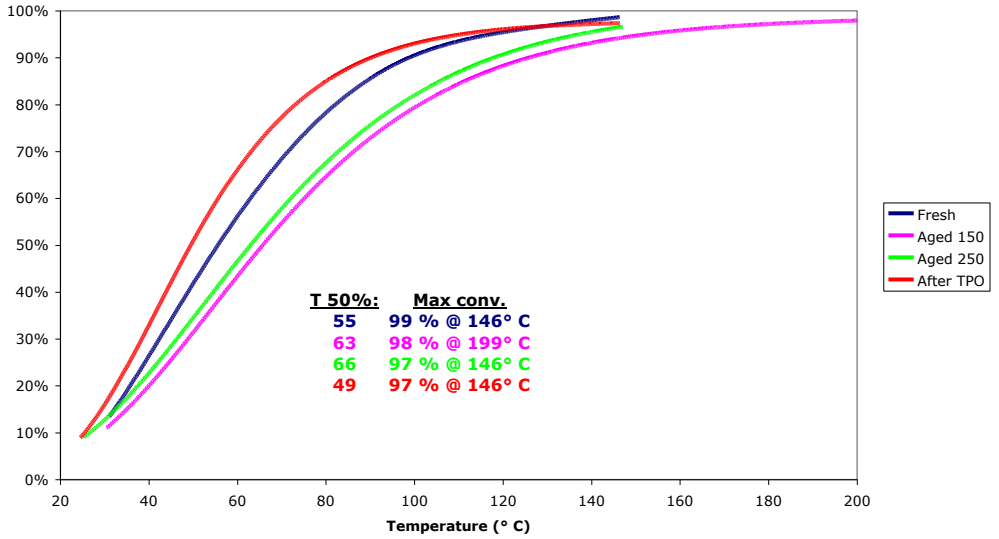

TPO = temperature programmed oxidation

M. Cargnello, C. Gentilini, T. Montini, E. Fonda, S. Mehraeen, M. Chi, M. Herrera-Collado, N. D. Browning, L. Pasquato, P. Fornasiero Chem. Mater. ***2010****, 22, 4335-4345.*

Synthesis of Dispersible Pd@CeO2 Core-Shell Nanostructures by Self-Assembly

Matteo Cargnello, Noah L. Wieder, Tiziano Montini, Raymond J. Gorte, and Paolo Fornasiero*, *J. AM. CHEM. SOC.* **2010**, *132*, 1402–1409

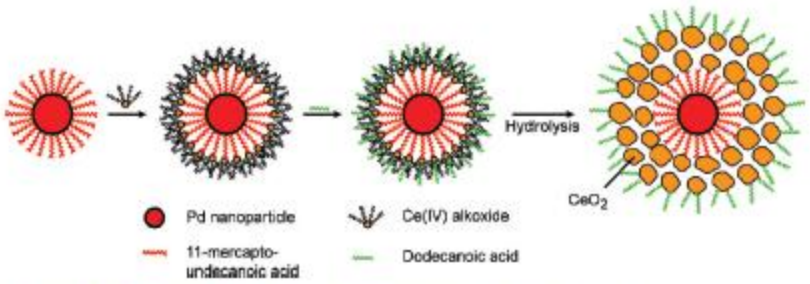

Figure 1. Schematic representation of the procedure to obtain dispersible Pd@CeO_2 core−shell nanostructures.

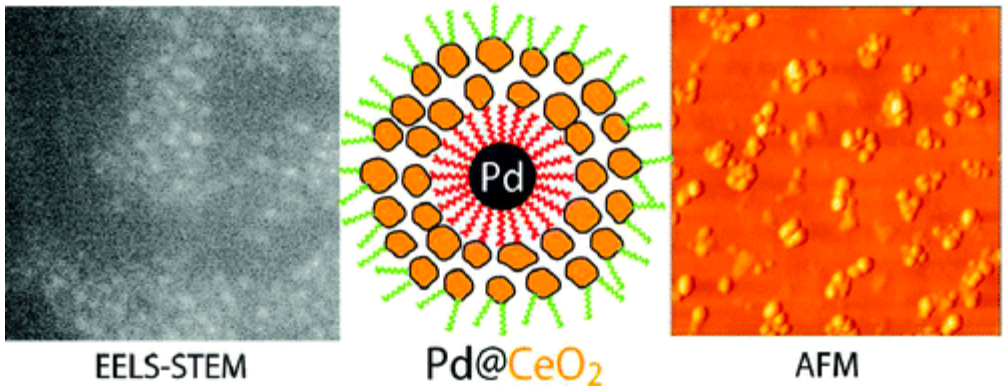

Exceptional Activity for Methane Combustion over Modular $Pd@CeO_2$ Subunits on Functionalized Al_2O_3

M. Cargnello,1 J. J. Delgado Jaén,2 J. C. Hernández Garrido,2 K. Bakhmutsky,3 T. Montini,1
J. J. Calvino Gámez,2 R. J. Gorte,3* P. Fornasiero1*SCIENCE VOL 337 10 AUGUST 2012

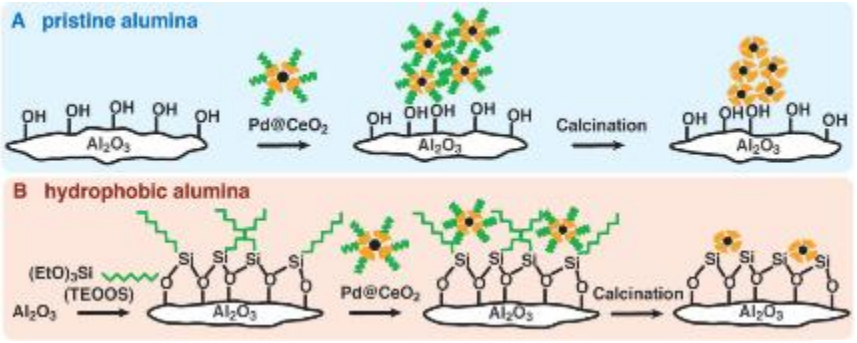

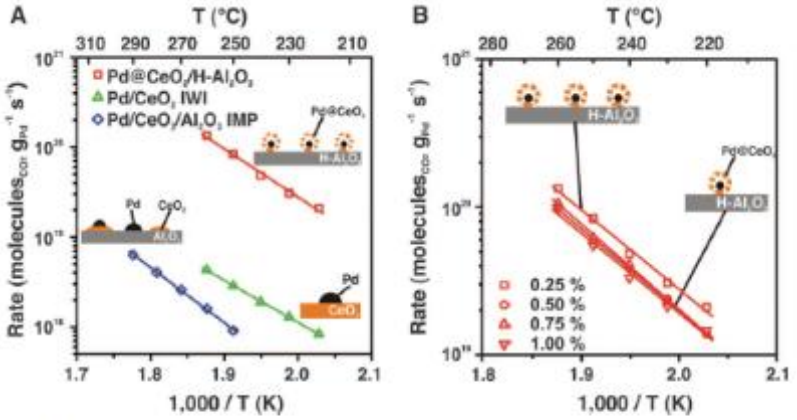

Fig. 4. Kinetic rate data for CH_4 oxidation on **(A)** $Pd@CeO_2/H\text{-}Al_2O_3$ core-shell catalyst, Pd/CeO_2-IWI, and $Pd/CeO_2/Al_2O_3$-IMP; **(B)** $Pd@CeO_2/H\text{-}Al_2O_3$ core-shell catalysts at different loadings of the structures (Pd/Ce weight ratio was kept at 1/9): Pd loading of 0.25, 0.50, 0.75, and 1.00%.

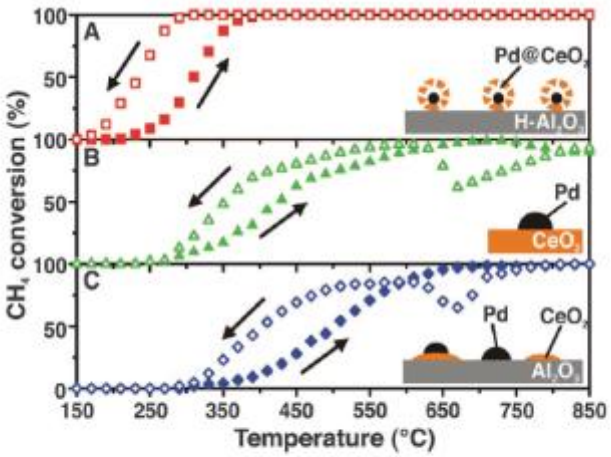

Fig. 3. Heating and cooling (10°C min^{-1}) light-off curves of CH_4 conversion against the temperature for the three catalyst formulations used. **(A)** $Pd@CeO_2/H\text{-}Al_2O_3$ core-shell catalyst, **(B)** Pd/CeO_2-IWI, and **(C)** $Pd/CeO_2/Al_2O_3$-IMP.

Imaging and Therapy

CT Imaging and Therapy of Prostate Cancer

loading of the trifunctional Au NPs with the chemoterapeutic drug Doxorubicin

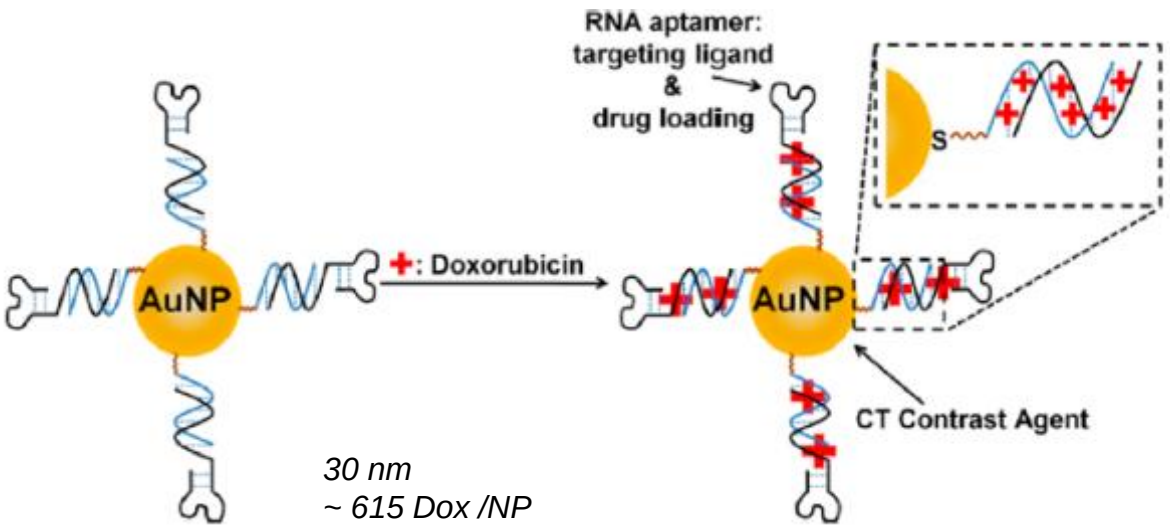

30 nm
~ 615 Dox /NP

doxorubicin

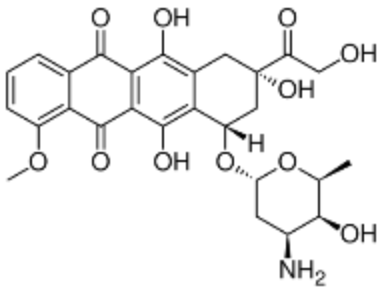

7.5 Dox per aptamer

prostate-specific membrane antigen-specific RNA aptamer target prostate adenocarcinoma LNCaP cells.

the gold center serves as the CT imaging agent, while the RNA aptamer modifications turn the NP into a target drug-delivery vehicle

*D. Kim, Y. Y. Jeong, S. Jon ACS Nano **2010**, 4, 3689.*

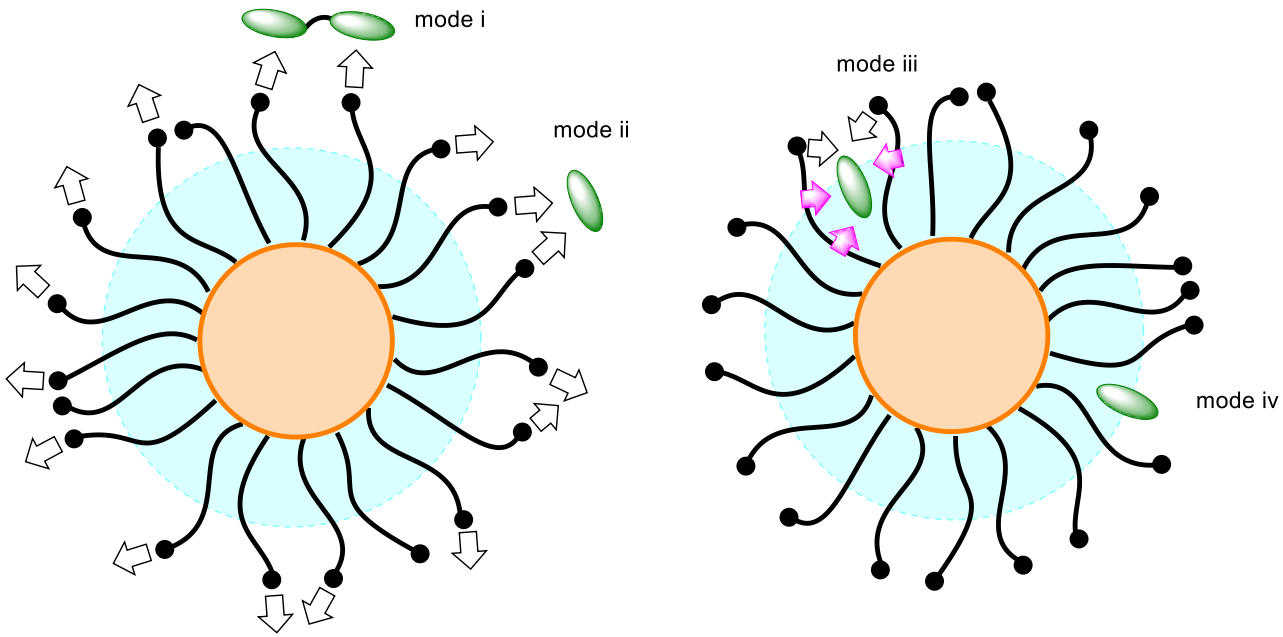

Possible binding modes by monolayer coated nanoparticles. Mode i: multivalent binding; mode ii: tweezer-like binding; iii) hydrophobic partition; iv) cleft-like binding.

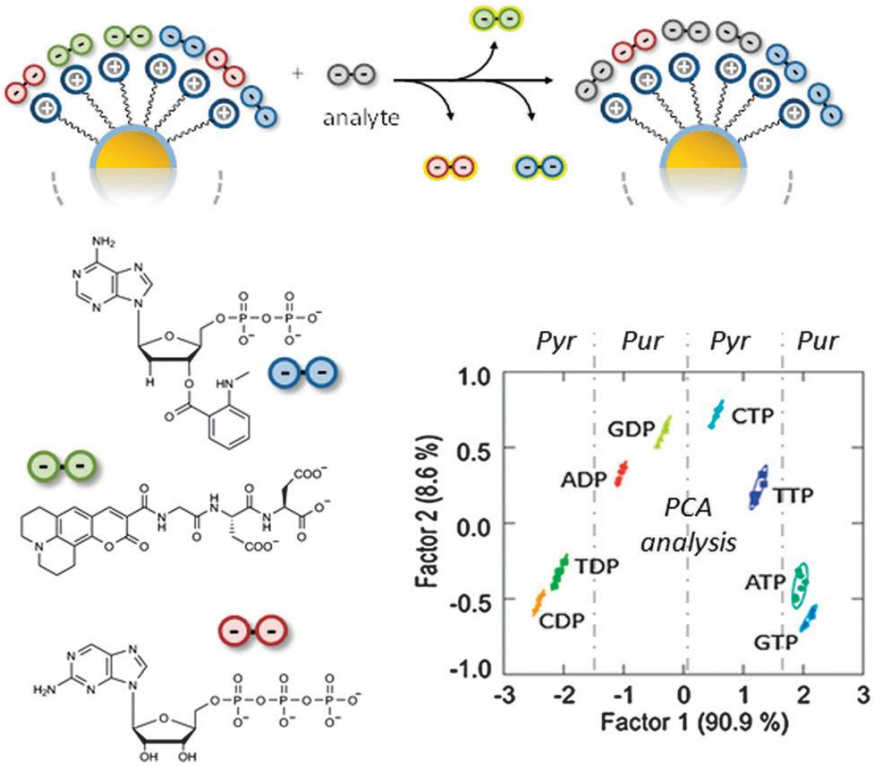

MPNs based sensing array studied by L.J. Prins and K. Severin

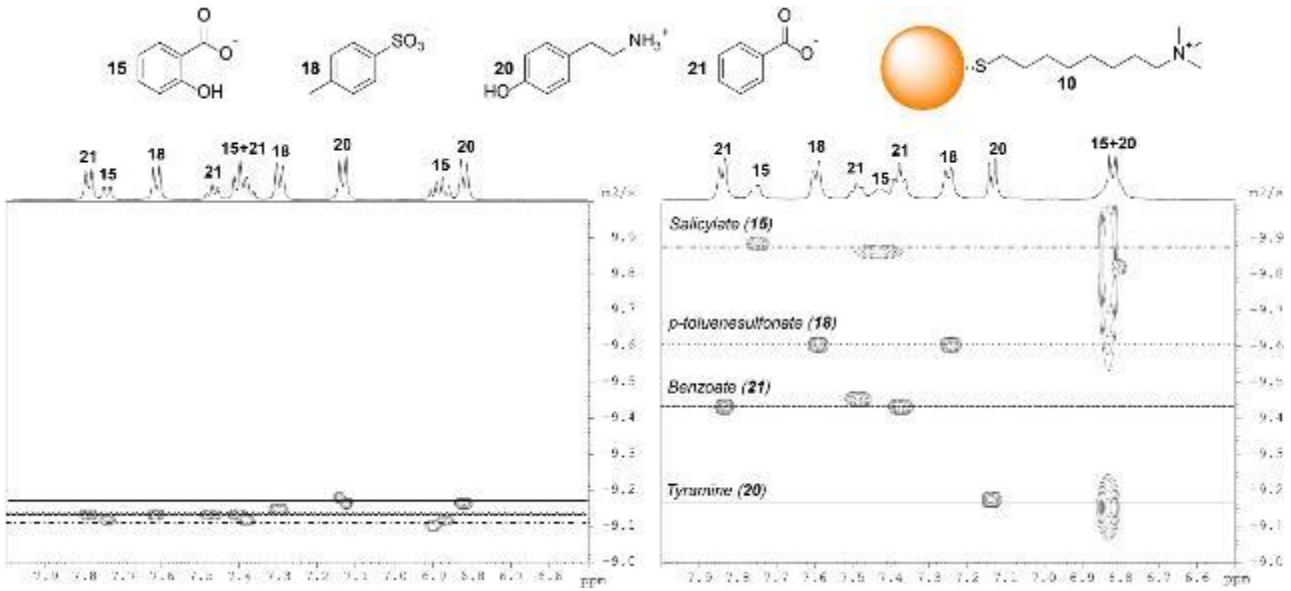

*^{1}H DOSY maps resulting from a mixture of sodium salicylate (**15**), potassium p-toluenesulfonate (**18**), sodium benzoate (**21**), and tyramine (**20**) in water in the absence (left) or in the presence (right) of nanoparticles coated with ammonium ligands.*

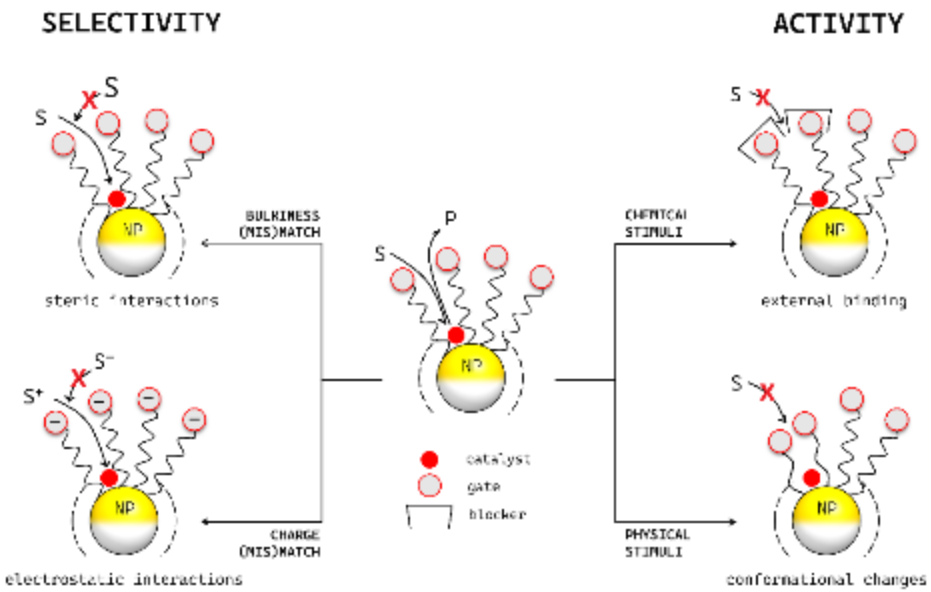

General strategies to the regulation of catalyst activity and selectivity within organic monolayers.

Chemoelectronic circuits based on metal nanoparticles

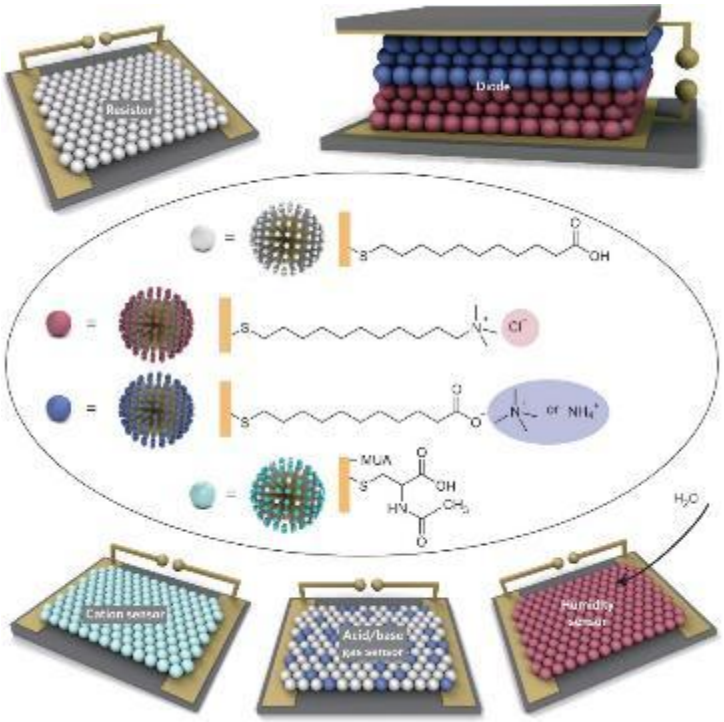

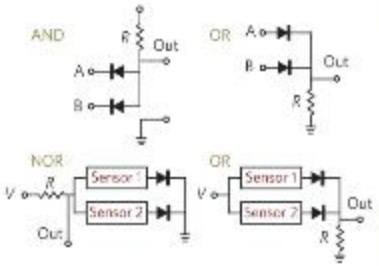

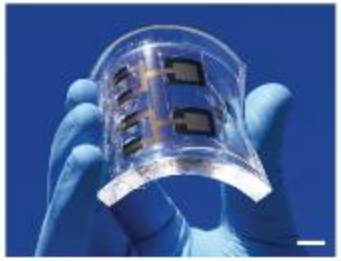

Chemoelectronic circuits based on metal nanoparticles.
The left portion shows the alkane thiol ligands used to coat 5.5 nm AuNPs to achieve various chemoelectronic functions. Nanoparticles functionalized with $(CH_2)_{11}$-$N(CH_3)_3^+$ ligands are surrounded by mobile Cl^- anions (red); nanoparticles covered with HS-$(CH_2)_{10}$-COO^- ligands and surrounded by mobile $N(CH_3)_4^+$ or NH_4^+ cations (blue); nanoparticles covered with HS-$(CH_2)_{10}$-COOH ligands (white); and nanoparticles covered with mixed SAMs of protonated MUA and HS-$CH_2CH(NHCOCH_3)COOH$ have no mobile ions (light cyan). Active layers of resistors, diodes, acid/base gas sensors, cation sensors and humidity sensors were assembled using these nanoparticles.
For clarity, the illustrations show a single layer of nanoparticles. In reality, the nanoparticle films are hundreds of nanometres thick. The scheme below shows architectures of various logic gates and gates combined with the sensing elements. The image on the right, right has an actual chemoelectronic circuit deposited and deformed on a PDMS substrate. Two golden “forks” house two sensors each (in duplicate), and the square elements are two diodes The diodes are fully embedded in PDMS, while the sensors have their top surfaces open to the atmosphere. Scale bar is 1 cm.

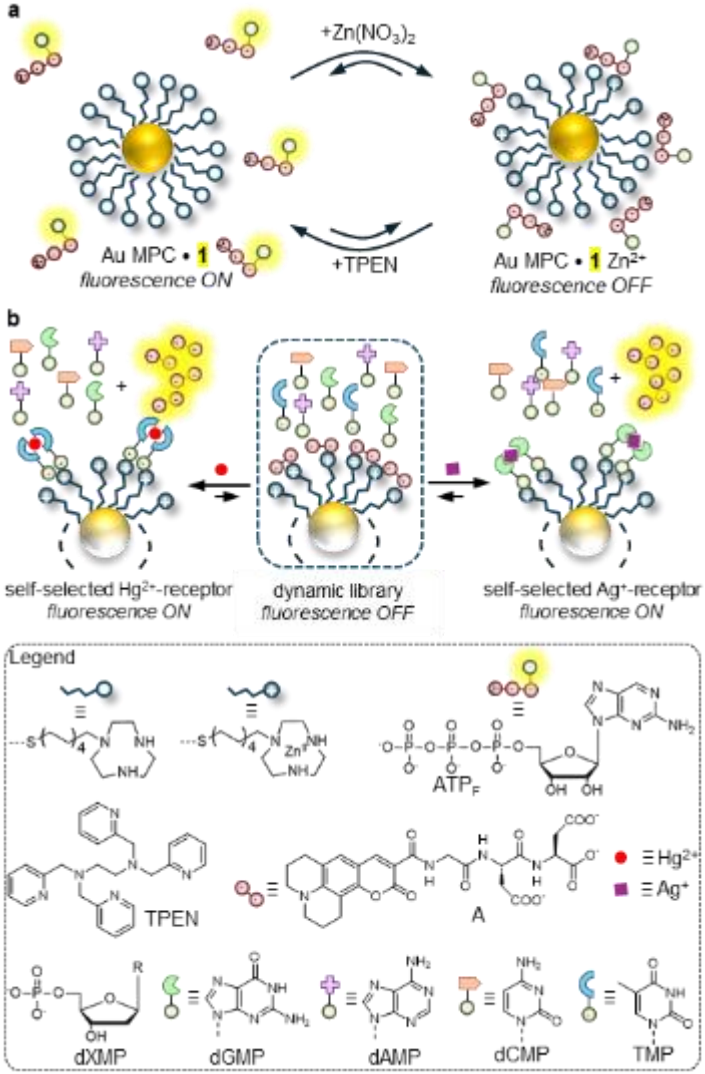

*a) Schematic representation of metal-mediated control over the valency of the nanoparticle-based supramolecular system. b) Schematic representation of metal-mediated self-selection: complex formation between two recognition units and a metal ion results in the formation of a ternary complex with a high affinity for Au MPC **1** • Zn^{2+}, resulting in the displacement of fluorescent probe **A** from the surface, activating its fluorescence.*